

Spin Photocurrents in Quantum Wells

review part I, (part II: cond-mat/one of the next numbers)

Sergey D. Ganichev and Wilhelm Prettl

Fakultät für Physik, Universität Regensburg, 93040 Regensburg, Germany,

ABSTRACT

Spin photocurrents generated by homogeneous optical excitation with circularly polarized radiation in quantum wells (QWs) are reviewed. The absorption of circularly polarized light results in optical spin orientation due to the transfer of the angular momentum of photons to electrons of a two-dimensional electron gas (2DEG). It is shown that in quantum wells belonging to one of the gyrotropic crystal classes a non-equilibrium spin polarization of uniformly distributed electrons causes a directed motion of electron in the plane of the QW. A characteristic feature of this electric current, which occurs in unbiased samples, is that it reverses its direction upon changing the radiation helicity from left-handed to right-handed and vice versa.

Two microscopic mechanisms are responsible for the occurrence of an electric current linked to a uniform spin polarization in a QW: the spin polarization induced circular photogalvanic effect and the spin-galvanic effect. In both effects the current flow is driven by an asymmetric distribution of spin polarized carriers in \mathbf{k} -space of systems with lifted spin degeneracy due to \mathbf{k} -linear terms in the Hamiltonian. Spin photocurrents provide methods to investigate spin relaxation and to conclude on the in-plane symmetry of QWs. The effect can also be utilized to develop fast detectors to determine the degree of circular polarization of a radiation beam. Furthermore spin photocurrents at infrared excitation were used to demonstrate and investigate monopolar spin orientation of free carriers.

Contents

1	Introduction	4
2	Homogeneous spin orientation induced photocurrents	5
2.1	Removal of spin degeneracy	6
2.1.1	\mathbf{k} -linear terms in the effective Hamiltonian	6
2.1.2	Spin splitting of energy bands in zinc-blende structure based QWs	7
2.2	Circular photogalvanic effect	9
2.2.1	Microscopic model	9
2.2.2	Phenomenology	11
2.2.3	Microscopic theory	13
2.2.4	One- and two-photon excitation	15
2.3	Spin-galvanic effect	15
2.3.1	Phenomenology	15
2.3.2	Microscopic model	16
2.3.3	Microscopic theory	17
2.3.4	Spin-galvanic effect at optical orientation	17
2.3.5	Spin-galvanic effect at optical orientation in the presence of magnetic field	18
2.4	Spin orientation induced circular photogalvanic effect versus spin-galvanic effect	19
3	Methods	19
3.1	Samples	19
3.2	Experimental technique	20

4	Experimental results and discussion	21
4.1	Spin polarization induced circular photogalvanic effect	21
4.1.1	General features	21
4.1.2	Inter-subband transitions in <i>n</i> -type QWs	23
4.1.3	Inter-subband transitions in <i>p</i> -type QWs	24
4.1.4	Intra-subband transitions in QWs	25
4.1.5	Spin orientation induced CPGE in SiGe QWs	25

please replace this page by the table of contents of part II

1 Introduction

The spin of electrons and holes in solid state systems is an intensively studied quantum mechanical property showing a large variety of interesting physical phenomena. Lately, there is much interest in the use of the spin of carriers in semiconductor heterostructures together with their charge to realize novel concepts like spintronics and several schemes of quantum computation (for review see [1]). The necessary conditions to realize spintronic devices are high spin polarizations in low dimensional structures and large spin-splitting of subbands in \mathbf{k} -space due to \mathbf{k} -linear terms in the Hamiltonian. The latter is important for the ability to manipulate spins with an external electric field by the Rashba effect [2]. Significant progress has been achieved recently in the injection of spin polarized electrons (or holes), in demonstrating the Rashba splitting and also in using the splitting for manipulating the spins [1].

One of the most frequently used and powerful methods of generation and investigation of spin polarization is optical orientation [3]. Optical generation of an unbalanced spin distribution in a semiconductor may lead to a spin photoconductive effect as well as to a spin photocurrent. In the spin photoconductive effect the optical spin orientation yields a change of conductivity which, at application of an external voltage bias, results in a spin polarized current [4–6]. On the other hand, spin photocurrents reviewed here occur without an external bias. They are electric currents which are driven by optically generated spin polarization.

A spin photocurrent was proposed for the first time in [7] (see also [8]) and thereafter observed in bulk AlGaAs [9]. In these works it was shown that an inhomogeneity of the spin polarization of electrons results in a surface current due to spin-orbit interaction. A gradient of spin density was obtained by making use of the strong fundamental absorption of circularly polarized light at the band edge of the semiconductor. This and other spin photocurrents caused by inhomogeneous spin orientation will be briefly outlined in section 6.

In the present paper we review a new property of the electron spin in a homogeneous spin-polarized two-dimensional electron gas: its ability to drive an electric current if some general symmetry requirements are met. Recently it was demonstrated that an optical excitation of quantum well structures with circularly polarized radiation leads to a current whose direction and magnitude depends on the degree of circular polarization of the incident light [10]. This effect belongs to the class of photogalvanic effects which were intensively studied in semiconductors (for review see [11–14]) and represents a circular photogalvanic effect (CPGE). The CPGE can be considered as a transfer of the photon angular momentum into a directed motion of a free charge carrier. It is an electronic analog of mechanical systems which transmit rotatory motion into linear one like a screw thread or a propeller. The circular photogalvanic effect was independently predicted by Ivchenko and Pikus [15] and Belinicher [16] and then observed in bulk tellurium [17,18] (for reviews see [13,14]). In tellurium the current arises due to spin splitting of the valence band edge at the boundary of the first Brillouin-zone (‘camel back’ structure) [19]. While neither bulk zinc-blende structure materials like GaAs and related compounds nor bulk diamond structure crystals like Si and Ge allow this effect, in QW structures CPGE is possible due to a reduction of symmetry.

It was shown in [20] that in zinc-blende structure based QW structures CPGE is caused by optical spin orientation of carriers in systems with band splitting in \mathbf{k} -space due to \mathbf{k} -linear terms in the Hamiltonian. Here \mathbf{k} is the two-dimensional electron wavevector in the plane of QW. In this case homogeneous irradiation of QWs with circularly polarized light results in a non-uniform distribution of photoexcited carriers in \mathbf{k} -space due to optical selection rules and energy and momentum conservation which leads to a current [20–26]. The carrier distribution in the real space remains uniform.

Furthermore, a thermalized but spin-polarized electron gas can drive an electrical current [27, 28]. Recently it was demonstrated that a homogeneous spin polarization obtained by any means, not necessarily optical, yields a current, if the same symmetry requirements, which allow \mathbf{k} -linear terms in the Hamiltonian, are met [29]. This phenomenon is referred to as spin-galvanic effect. While electrical currents are usually generated by electric or magnetic fields or gradients, in this case a uniform non-equilibrium population of electron spins gives rise to an electric current. The microscopic origin of the spin-galvanic effect is an inherent asymmetry of spin-flip scattering of electrons in systems with removed \mathbf{k} -space spin degeneracy of the band structure. This effect has been demonstrated by optical spin orientation [29–31] and therefore also represents a spin

photocurrent.

Both spin orientation induced CPGE and the spin-galvanic effect in QWs occur at one-photon excitation yielding an electric charge current linked to a spin polarization. However, a pure spin current may be obtained at simultaneous one- and two-photon coherent excitation of proper polarization as recently demonstrated in bulk GaAs [32, 33]. This phenomenon may be attributed to a photogalvanic effect where the reduced symmetry is caused by the coherent two-frequency excitation [34] which may also occur in QWs [35].

Spin photocurrents at homogeneous excitation have been observed in *n*- and *p*-type quantum wells based on various semiconductor materials at very different types of optical excitation by application of several lasers at wavelengths ranging from the visible to the far-infrared. There is a particular interest in spin photocurrents generated by infrared radiation because, in contrast to conventional methods of optical spin orientation using inter-band transitions [3], only one type of charge carriers is excited yielding monopolar spin orientation [29, 36–41]. Therefore infrared spin orientation allows to study spin relaxation without electron-hole interaction and exciton formation at conditions close to the case of electrical spin injection [29, 38, 39]. Finally, spin photocurrents have found technical application as room temperature detectors which allow to determine and monitor the state of polarization of terahertz radiation with picosecond time resolution [42].

This paper is organized in the following way: in section 2 an overview of mechanisms yielding photocurrents at homogeneous spin orientation in QWs is given. First the removal of spin degeneracy due to spin-orbit interaction in QWs is discussed and then it is shown that spin splitting in *k*-space is the basic reason for different mechanisms of spin photocurrents in QWs. Section 3 gives a short account of the experimental technique. In section 4 the experimental results are presented and discussed in view of the theoretical background. Section 5 sketches several kinds of spin independent photocurrents in comparison to spin photocurrents and experimental methods are introduced allowing to distinguish between spin dependent and spin independent currents. Finally, in section 6 we present several mechanisms of spin photocurrents due to inhomogeneities.

2 Homogeneous spin orientation induced photocurrents

Light propagating through a semiconductor and acting upon mobile carriers can generate a *dc* electric current without external bias. The irradiated sample represents a current source. Here we consider photocurrents which appear due to optically induced homogeneous spin orientation of carriers in homogeneous samples. The microscopic origin of these currents is the conversion of spin polarization of carriers into directed motion. The fingerprint of spin photocurrents is their dependence on the helicity of the radiation field. The current reverses its direction by switching the polarization of light from right-handed circular to left-handed circular and vice versa. The experimental data can be described by simple analytical expressions derived from a phenomenological theory which shows that the effect can only be present in gyrotropic media. This requirement rules out effects depending on the helicity of the radiation field in bulk non-optically active materials like bulk zinc-blende structure and diamond structure crystals. The reduction of dimensionality as realized in QWs makes spin photocurrents possible. The effect is quite general and has so far been observed in GaAs [10, 20, 29, 38], InAs [20, 29, 30], BeZnMnSe [43] QW structures, and in asymmetric SiGe QWs [23].

On a microscopical level spin photocurrents are the result of spin orientation in systems with *k*-linear terms in the Hamiltonian which also may occur in gyrotropic media only. In general, two mechanisms contribute to spin photocurrents: photoexcitation and scattering of photoexcited carriers. The first is spin orientation induced circular photogalvanic effect which is caused by the asymmetry of the momentum distribution of carriers excited in optical transitions which are sensitive to the light circular polarization due to selection rules [20]. The second mechanism is the spin-galvanic effect which is a result of spin relaxation. In general this effect does not need optical excitation but may also occur due to optical spin orientation [29]. The current caused by CPGE is spin polarized and decays with the momentum relaxation time of free carriers whereas the spin-galvanic effect induced current is unpolarized but decays with the spin relaxation time.

2.1 Removal of spin degeneracy

2.1.1 \mathbf{k} -linear terms in the effective Hamiltonian

Quantum phenomena in semiconductors are highly sensitive to subtle details of the carrier energy spectrum so that even a small spin splitting of energy bands may result in measurable effects. Spin dependent terms linear in the wavevector \mathbf{k} in the effective Hamiltonian remove the spin degeneracy in \mathbf{k} -space of the carrier spectrum. The presence of these terms in QWs gives rise to spin photocurrents, yields beating patterns in Shubnikov-de-Haas oscillations [2, 44, 45], determines spin relaxation in QWs [1, 46, 47], results in spin-polarized tunnelling [48–51], and allows the control of spin orientation by external fields [1, 2, 52–58].

In the general case, the terms linear in \mathbf{k} appear because the symmetry of heterostructures is lower than the symmetry of the corresponding bulk materials. Spin degeneracy of electron bands in semiconductors and subbands of heterostructures results because of simultaneous presence of time reversal and spatial inversion symmetry. In the present case of low dimensional heterostructures and quantum wells, the spatial inversion symmetry is broken. However, in order to obtain spin photocurrents depending on the helicity of radiation and spin orientation, inversion asymmetry is a necessary, but not a sufficient condition. As a matter of fact, the materials must belong to one of the gyrotropic crystal classes which have second rank pseudo-tensors as invariants. As a consequence spin dependent \mathbf{k} -linear terms caused by spin-orbit interaction appear in the electron Hamiltonian leading to a splitting of electronic subbands in \mathbf{k} -space. As long as the time reversal symmetry is not broken by the application of an external magnetic field, the degeneracy of Kramers doublets is not lifted so that still $\varepsilon(\mathbf{k}, \uparrow) = \varepsilon(-\mathbf{k}, \downarrow)$. Here ε is the electron energy and the arrows indicate the spin orientation.

The principal sources of \mathbf{k} -linear terms in the band structure of QWs are the bulk inversion asymmetry (BIA) of zinc-blende structure crystals and possibly a structural inversion asymmetry (SIA) of the low dimensional quantizing structure (see [1, 2, 23, 46–80] and references therein). In addition an interface inversion asymmetry (IIA) may yield \mathbf{k} -linear terms caused by non-inversion symmetric bonding of atoms at heterostructure interfaces [1, 23, 81–87].

BIA induces \mathbf{k} -linear terms in the 2D Hamiltonian, known as Dresselhaus terms, due to the absence of an inversion center in the bulk crystal. The Dresselhaus terms originate from the \mathbf{k} -cubic terms in the Hamiltonian of a bulk material [88]. Averaging these cubic terms along the quantization axis in the case of low subband filling with carriers gives rise to the terms linear in \mathbf{k} . These terms are present in QWs based on zinc-blende structure material and are absent in SiGe heterostructures. IIA may occur in zinc-blende structure based QWs [81–86] where the well and the cladding have different compositions of both anions and cations like an InAs/GaSb QWs as well as in SiGe [23, 87]. IIA yields BIA-like terms in the effective Hamiltonian [23, 87], thus on a phenomenological level a separation between BIA and IIA is not necessary.

The SIA contribution to the removal of spin degeneracy is caused by the intrinsic heterostructure asymmetry which needs not to be related to the crystal lattice. These \mathbf{k} -linear terms in the Hamiltonian were first recognized by Rashba and are called Rashba terms [2, 89]. SIA may arise from different kinds of asymmetries of heterostructures like non-equivalent normal and inverted interfaces, asymmetric doping of QWs, asymmetric shaped QWs, external or built-in electric fields etc. and may also exist in QWs prepared from materials with inversion symmetry like Si and Ge [23, 86]. It is the SIA term which allows control of spin polarization by externally applied electric fields [2]. Therefore these spin-orbit coupling terms are important for spintronics and in particular for the spin transistor [90].

In the unperturbed symmetric case we will assume a doubly degenerated subband. Then the spin-orbit coupling in the non-symmetric structure has the form

$$\hat{H}' = \sum_{lm} \beta_{lm} \sigma_l k_m \quad (1)$$

where β_{lm} is a second rank pseudo-tensor and σ_l are the Pauli-matrices. The Pauli matrices occur here because of time reversal symmetry.

In Eq. (1) BIA, IIA and SIA can be distinguished by decomposing $\sigma_l k_m$ into a symmetric and an anti-symmetric product:

$$\sigma_l k_m = \{\sigma_l, k_m\} + [\sigma_l, k_m] \quad (2)$$

with the symmetric term

$$\{\sigma_l, k_m\} = \frac{1}{2} (\sigma_l k_m + \sigma_m k_l) \quad (3)$$

and the anti-symmetric term

$$[\sigma_l, k_m] = \frac{1}{2} (\sigma_l k_m - \sigma_m k_l). \quad (4)$$

Now the perturbation can be written as:

$$\hat{H}' = \sum_{lm} (\beta_{lm}^s \{\sigma_l k_m\} + \beta_{lm}^a [\sigma_l k_m]) \quad (5)$$

where β_{lm}^s and β_{lm}^a are symmetric and anti-symmetric pseudo-tensors projected out of the full tensor by the symmetric and anti-symmetric products of $\sigma_l k_m$, respectively. The symmetric term describes BIA as well as possible IIA-terms whereas the anti-symmetric term is caused by SIA.

2.1.2 Spin splitting of energy bands in zinc-blende structure based QWs

The pseudo-tensor β_{lm} as a material property must transform after the identity representation of the point group symmetry of the quantum well. The point group is determined by the crystallographic orientation and the profile of growth and doping of QWs. The three point groups D_{2d} , C_{2v} and C_s are particularly relevant for zinc-blende structure based QW [14]. Hereafter the Schönflies notation is used to label the point groups. In the international notation they are labelled as $\bar{4}2m$, $mm2$ and m , respectively. The D_{2d} point-group symmetry corresponds to perfectly grown (001)-oriented QWs with symmetric doping. In such QWs only BIA and IIA terms may exist. The symmetry of (001)-grown QWs reduces from D_{2d} to C_{2v} if an additional asymmetry is present due to e.g. non-equivalent interfaces, asymmetric growth profiles, asymmetric doping etc. resulting in SIA. The relative strength of BIA, IIA and SIA depends on the structure of the quantum well. In structures of strong growth direction asymmetry like heterojunctions the SIA term may be larger than that of BIA and IIA. The last point group is C_s , which contains only two elements, the identity and one mirror reflection plane. It is realized for instance in (113)- and miscut (001)- oriented samples.

The non-zero components of the pseudo-tensor β_{lm} depend on the symmetry and the coordinate system used. For (001)-crystallographic orientation grown QWs of D_{2d} and C_{2v} symmetry the tensor elements are given in the coordinate system (xyz) with $x \parallel [1\bar{1}0]$, $y \parallel [110]$, $z \parallel [001]$. The coordinates x and y are in the reflection planes of both point groups perpendicular to the principle two fold axis; z is along the growth direction normal to the plane of the QW. In D_{2d} the pseudo-tensor β_{lm} is symmetric, $\beta_{lm} = \beta_{lm}^s$. In the above coordinate system there are two non-zero components β_{xy} and β_{yx} with $\beta_{yx} = \beta_{xy} = \beta_{xy}^s$. For zinc-blende structure type crystals it has been shown that the BIA and IIA terms in the Hamiltonian have the same form, thus, IIA enhances or reduces the strength of BIA-like term.

Therefore we obtain¹

$$\hat{H}' = \hat{H}_{BIA} + \hat{H}_{IIA} = \beta_{xy}^s (\sigma_x k_y + \sigma_y k_x) \quad (6)$$

In C_{2v} the tensor β_{lm} is non-symmetric yielding additional terms in \hat{H}' caused by SIA so that now $\hat{H}' = \hat{H}_{BIA} + \hat{H}_{IIA} + \hat{H}_{SIA}$. The form of \hat{H}_{BIA} and \hat{H}_{IIA} remains unchanged by the reduction of symmetry from D_{2d} to C_{2v} . The SIA term in C_{2v} assumes the form:

$$\hat{H}_{SIA} = \beta_{xy}^a (\sigma_x k_y - \sigma_y k_x). \quad (7)$$

It is clear that the form of this term is independent of the orientation of cartesian coordinates in the plane of the QW. The strength of spin splitting was experimentally derived e.g. from beatings of

¹For coordinates along cubic axes, $x \parallel [100]$ and $y \parallel [010]$, we have non-zero components β_{xx} and β_{yy} with $\beta_{yy} = -\beta_{xx}$ which yields $\hat{H}' = \hat{H}_{BIA} + \hat{H}_{IIA} = \beta_{xx} (\sigma_x k_x - \sigma_y k_y)$.

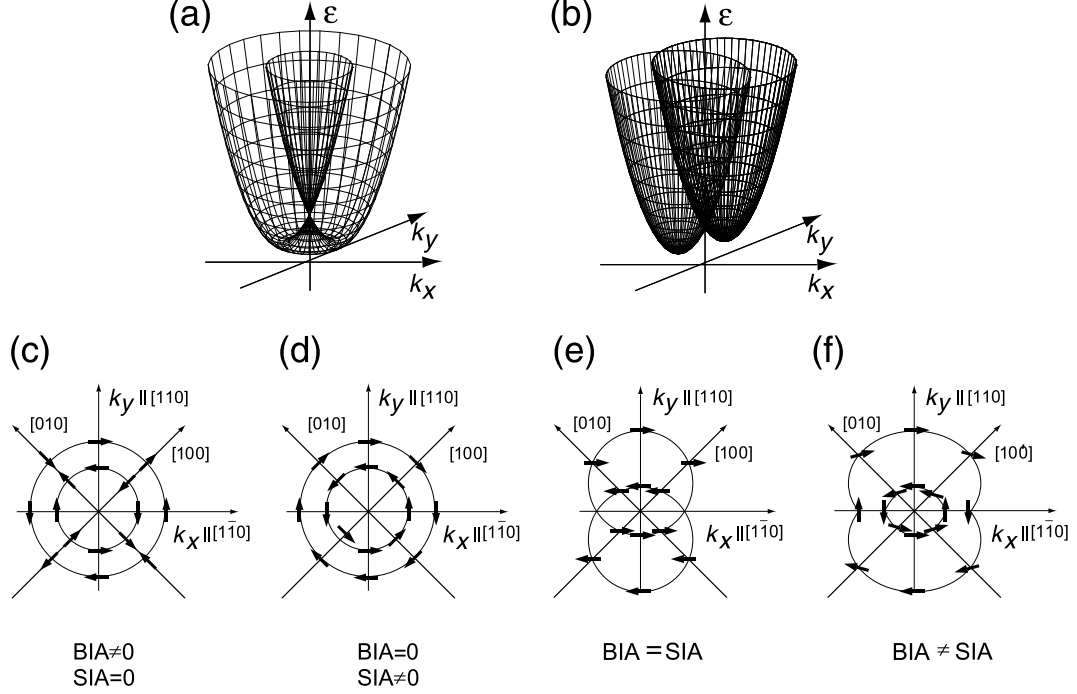


Figure 1: Schematic 2D band structure with \mathbf{k} -linear terms for C_{2v} symmetry. The energy ε is plotted as a function of k_x and k_y in (a) with only one type of inversion asymmetry, BIA or SIA, respectively and in (b) for equal strength of the BIA and SIA terms in the Hamiltonian. The bottom plate shows the distribution of spin orientations at the 2D Fermi energy for different strength of the BIA and SIA terms.

Shubnikov-de-Haas oscillations in various III-V-compound based QWs [2,44,45]. It has been found to be in the range of 10^{-10} and 10^{-9} eV·cm and was attributed to structural inversion asymmetry.

The point group C_s is discussed by example of (113)-orientation grown QWs because they are available and spin photocurrents in them have been intensively investigated so far². In this case we use the coordinates $x' = x \parallel [1\bar{1}0]$, as above, $y' \parallel [33\bar{2}]$, $z' \parallel [113]$. Direction x is normal to the reflection plane, the only non-identity symmetry element of this group, and z' is along the growth direction. The reduction of the symmetry to C_s results in an additional term in the Hamiltonian:

$$\hat{H}' = \beta_{z'x} \sigma_{z'} k_x. \quad (8)$$

In order to illustrate band structures with a \mathbf{k} -linear term in Fig. 1 we plotted the energy ε as a function of k_x and k_y for C_{2v} symmetry. The upper plate of Fig. 1 shows the band structure with only one type of inversion asymmetry, BIA or SIA (Fig. 1a) and the band structure at equal strength of the BIA (including IIA) and SIA (Fig. 1b). In the illustration we assume positive coefficients $\beta_{lm}^a, \beta_{lm}^s \geq 0$. In the case of BIA only ($\beta_{lm}^a = 0$) or SIA only ($\beta_{lm}^s = 0$) the band structure is the result of the revolution around the energy axis of two parabolas symmetrically displaced with respect to $\mathbf{k} = 0$. A constant energy surface is a pair of concentric circles, however, the spins are oriented differently for BIA and SIA. The distribution of spin orientation in \mathbf{k} -space, obtained by the procedure of [68], is indicated by arrows in the bottom plate of Fig. 1. The distribution of spins for a pure BIA term is shown in Fig. 1c. If only the SIA term is present (Fig. 1d) then the spins are always oriented normal to the wavevector \mathbf{k} . This is a consequence of the vector product in the Rashba spin-orbit interaction [2]. If the strengths of BIA and SIA are the same then the 2D band structure consists of two revolution paraboloids with revolution axes symmetrically shifted in opposite direction with respect to $\mathbf{k} = 0$ (Fig. 1b). Now the spins are oriented along $\pm k_x$ as shown in Fig. 1e. In Fig. 1f we have shown a constant energy surface and direction of spins for $\beta_{lm}^a \neq \beta_{lm}^s$.

Finally we briefly discuss QWs prepared on SiGe. As both Si and Ge possess inversion centers there is no BIA, however both IIA, with BIA-like form of the Hamiltonian, and SIA may lead to

²Miscut (001)-oriented samples investigated in [10] also have C_s symmetry.

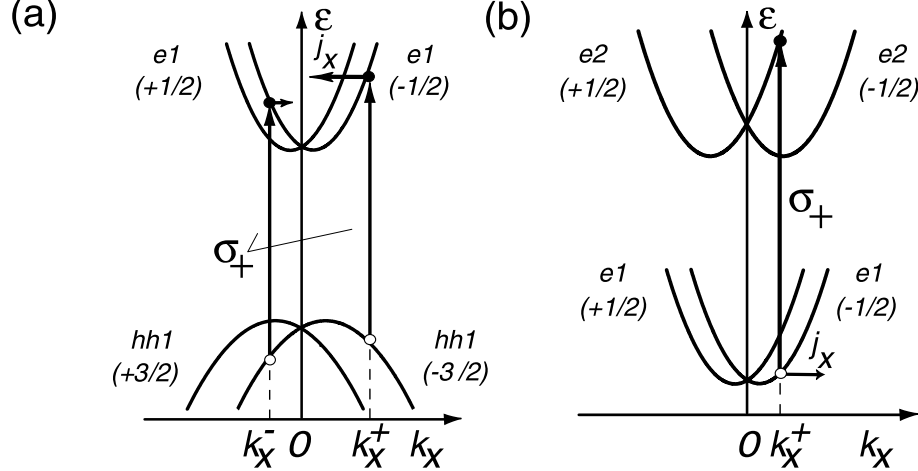


Figure 2: Microscopic picture of spin orientation induced CPGE at direct transitions in C_s point group taking into account the splitting of subbands in \mathbf{k} -space. σ_+ excitation induces direct transitions (solid arrows) (a) between valence and conduction band (from $hh1$ ($m_s = -3/2$) to $e1$ ($m_s = -1/2$)) and (b) between size quantized subbands in the conduction band (from $e1$ ($m_s = -1/2$) to $e2$ ($m_s = +1/2$)). Spin splitting together with optical selection rules results in an unbalanced occupation of the positive k_x^+ and negative k_x^- states yielding a spin polarized photocurrent. For σ_- excitation both the spin orientation of the charge carriers and the current direction get reversed. In each plate arrows indicate the current due to an unbalance of carriers. Currents are shown for one subband only.

\mathbf{k} -linear terms [23, 79, 86, 87]. The symmetry of $\text{Si}/(\text{Si}_{1-x}\text{Ge}_x)_n/\text{Si}$ QW depends on the number n of the monoatomic layers in the well. In the case of (001)-crystallographic orientation grown QW structures with an even number n , the symmetry of QWs is D_{2h} which is inversion symmetric and does not yield \mathbf{k} -linear terms. An odd number of n , however, interchanges the $[1\bar{1}0]$ and $[110]$ axes of the adjacent barriers and reduces the symmetry to D_{2d} with the same implication treated above for zinc-blende structure QWs [23].

2.2 Circular photogalvanic effect

2.2.1 Microscopic model

Inter-band transitions: The spin orientation induced circular photogalvanic effect is most easily conceivable for both n - and p -type materials from the schematic band structure shown in Fig. 2a [20]. We assume direct inter-band transitions in a QW of C_s symmetry. For the sake of simplicity we take into account a one dimensional band structure consisting only of the lowest conduction subband $e1$ and the highest heavy-hole subband $hh1$. The splitting in the conduction band is given by $\varepsilon_{e1,\pm 1/2}(\mathbf{k}) = [(\hbar^2 k_x^2/2m_{e1}) \pm \beta_{e1}k_x + \varepsilon_g]$ and in the valence band by $\varepsilon_{hh1,\pm 3/2}(\mathbf{k}) = -[(\hbar^2 k_x^2/2m_{hh1}) \pm \beta_{hh1}k_x]$, where ε_g is the energy gap.

For absorption of circularly polarized radiation of photon energy $\hbar\omega$ energy and momentum conservation allow transitions only for two values of k_x . Due to selection rules the optical transitions occur from $m_s = -3/2$ to $m_s = -1/2$ for right handed circular polarization (σ_+) and from $m_s = 3/2$ to $m_s = 1/2$ for left handed circular polarization (σ_-). Here m_s are the spin quantum numbers of the electron states. The corresponding transitions for e.g. σ_+ photons occur at

$$k_x^\pm = +\frac{\mu}{\hbar^2}(\beta_{e1} + \beta_{hh1}) \pm \sqrt{\frac{\mu^2}{\hbar^4}(\beta_{e1} + \beta_{hh1})^2 + \frac{2\mu}{\hbar^2}(\hbar\omega - \varepsilon_g)}, \quad (9)$$

and are shown in Fig. 2a by the solid vertical arrows. Here $\mu = (m_{e1} \cdot m_{hh1})/(m_{e1} + m_{hh1})$ is a reduced mass. The ‘center of mass’ of these transitions is shifted from the point $k_x = 0$ by $(\beta_{e1} + \beta_{hh1})(\mu/\hbar^2)$. Thus the sum of the electron velocities in the excited states in the conduction

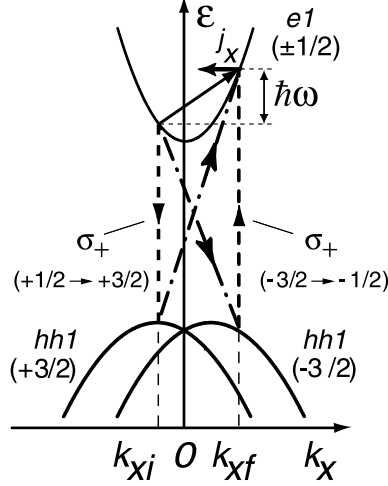


Figure 3: Microscopic picture describing the origin of spin orientation induced CPGE at indirect (Drude) transitions in C_s point group samples.

band, $v_{e1} = \hbar(k_x^- + k_x^+ - 2k_x^{min})/m_{e1} = 2/[\hbar(m_{e1} + m_{hh1})] \cdot (\beta_{hh1}m_{hh1} - \beta_{e1}m_{e1})$, is non-zero. The contributions of k_x^\pm photoelectrons to the current do not cancel each other except in the case of $\beta_{e1}m_{e1} = \beta_{hh1}m_{hh1}$ which corresponds to an equal splitting of the conduction and the valence band. We note that the group velocity is obtained taken into account that k_x^\pm are to be counted from the conduction subband minima k_x^{min} because the current is caused by the difference of the group velocities within the subband. The same consideration applies for holes in the initial states in $hh1$. Consequently, a spin polarized net current in the x direction results. Changing the circular polarization of the radiation from σ_+ to σ_- reverses the current because the ‘center of mass’ of these transitions is now shifted to $-(\beta_{e1} + \beta_{hh1})(\mu/\hbar^2)$.

Inter-subband transitions: In the longer wavelength range, infrared or far-infrared, the current is caused by inter- or intra-subband transition. For direct transition between size quantized states in the valence or conduction band, for example like $e1$ and $e2$ in n -type materials, the model is very similar to inter-band transitions discussed above [24]. In Fig. 2b we shortly sketch this situation for QWs of C_s symmetry. The $\sigma_z k_x$ contribution to the Hamiltonian splits the electron spectrum into spin sub-levels with the spin components $m_s = \pm 1/2$ along the growth direction z' . As a result of optical selection rules right-handed circular polarization under normal incidence induces direct optical transitions between the subband $e1$ with spin $m_s = -1/2$ and $e2$ with spin $m_s = +1/2$. For monochromatic radiation optical transitions occur only at a fixed k_x^\pm where the energy of the incident light matches the transition energy as is indicated by the arrow in Fig. 2b. Therefore optical transitions induce an imbalance of momentum distribution in both subbands yielding an electric current in the x direction with contributions from $e1$ and $e2$. As in n -type QWs the energy separation between $e1$ and $e2$ is typically larger than the energy of longitudinal optical phonons $\hbar\omega_{LO}$, the non-equilibrium distribution of electrons in $e2$ relaxes rapidly due to emission of phonons. As a result, the contribution of the $e2$ subband to the electric current vanishes. Thus the magnitude and the direction of the current is determined by the group velocity and the momentum relaxation time τ_p of photogenerated holes in the initial state of the resonant optical transition in the $e1$ subband with $m_s = -1/2$.

Intra-subband transitions (Drude absorption): Now we consider indirect intra-subband transitions. This situation is usually realized in the far-infrared range where the photon energy is not high enough to excite direct inter-subband transitions. Due to energy and momentum conservation intra-subband transitions can only occur by absorption of a photon and simultaneous absorption or emission of a phonon. This process is described by virtual transitions involving intermediate states and will be discussed in more detail in section 4.3.2. It can be shown that transitions via intermediate states within one and the same subband do not yield spin orientation and do not contribute to the spin photocurrent. However, spin selective indirect optical transitions excited by circularly polarized light with both initial and final states in the conduction band can generate

a spin current if virtual processes involve intermediate states in different subbands [20]. Fig. 3 sketches the underlying mechanism for σ_+ polarization. For the sake of simplicity only the spin splitting of the valence band is taken into account. The two virtual transitions shown represent excitations which, for σ_+ helicity, transfer electrons from states with negative k_x to states with positive k_x . The current resulting from a free electron transition (solid arrow) in the conduction band $e1$ occurs due to transitions involving intermediate states in the valence subbands. Two representative virtual transitions for σ_+ excitation are illustrated in Fig. 3. One is an optical transition from $m_s = +1/2$ to $m_s = +3/2$ (dashed line, downward arrow) and a transition involving a phonon from $m_s = +3/2$ back to the conduction band (dash-dotted line, upward arrow). The other is a phonon transition from the conduction band to the $m_s = -3/2$ intermediate state in $hh1$ and an optical transition from $m_s = -3/2$ to $m_s = -1/2$. While the first route depopulates preferentially initial states of spin $m_s = +1/2$ for $k_{xi} < 0$, the second one populates preferentially final state of $m_s = -1/2$ states for $k_{xf} > 0$ [20]. This together with the unbalanced occupation of the \mathbf{k} -space causes a spin-polarized photocurrent. Switching the helicity from σ_+ to σ_- reverses the process and results in a spin photocurrent in the opposite direction.

2.2.2 Phenomenology

On the macroscopic level the CPGE can be described by the following phenomenological expression [14]:

$$j_\lambda = \sum_\mu \gamma_{\lambda\mu} i(\mathbf{E} \times \mathbf{E}^*)_\mu, \quad (10)$$

$$i(\mathbf{E} \times \mathbf{E}^*)_\mu = \hat{e}_\mu E_0^2 P_{circ} \quad (11)$$

where \mathbf{j} is the photocurrent density, γ is a second rank pseudo-tensor, \mathbf{E} is the complex amplitude of the electric field of the electromagnetic wave, E_0 , P_{circ} , $\hat{\mathbf{e}} = \mathbf{q}/q$ and \mathbf{q} are the electric field amplitude, the degree of circular polarization, the unit vector pointing in the direction of light propagation and the light wavevector inside the medium, respectively. The photocurrent is proportional to the radiation helicity P_{circ} and can be observed only under circularly polarized excitation. The helicity of the incident radiation is given by

$$P_{circ} = \frac{I_{\sigma_+} - I_{\sigma_-}}{I_{\sigma_+} + I_{\sigma_-}} = \sin 2\varphi \quad (12)$$

where φ is the phase angle between the x and y component of the electric field vector. P_{circ} varies from -1 (left-handed circular, σ_-) to $+1$ (right-handed circular, σ_+).

In general, in addition to the circular photogalvanic current given in Eq. (10), two other photocurrents can be simultaneously present, namely the linear photogalvanic effect (LPGE) and the photon drag effect. Both effects were observed in low dimensional structures. They do not require spin orientation and will be summarized in section 5.

As a result of tensor equivalence the second rank pseudo-tensor γ is subjected to the same symmetry restriction as β responsible for the \mathbf{k} -linear terms in the Hamiltonian, discussed in detail above. Thus, γ_{lm} depends in the same way like β_{lm} on the symmetry and the coordinate system. In the various crystal classes being of importance here, the same elements of β_{lm} are non-zero like those of γ_{lm} .

In the following we analyze Eq. (10) for D_{2d} , C_{2v} and C_s in the coordinate systems (xyz) and $(xy'z')$. Due to carrier confinement in growth direction the photocurrent in QWs has non-vanishing components only in the plane of a QW.

For the point group D_{2d} the non-zero components of γ are γ_{xy} and γ_{yx} with $\gamma_{xy} = \gamma_{yx}$. We denote the only independent element by $\gamma^{(0)} = \gamma_{xy}$; then the current in a QW is given by:

$$j_x = \gamma^{(0)} \hat{e}_y E_0^2 P_{circ}, \quad j_y = \gamma^{(0)} \hat{e}_x E_0^2 P_{circ}. \quad (13)$$

where E_0^2 is the square of the electric field amplitude in vacuum being proportional to the radiation power P .

Eqs. (13) shows that in this configuration we get a transverse effect if the sample is irradiated along a $\langle 110 \rangle$ crystallographic orientation, corresponding to $\hat{e}_x = 1$, $\hat{e}_y = 0$ or $\hat{e}_x = 0$, $\hat{e}_y = 1$. The

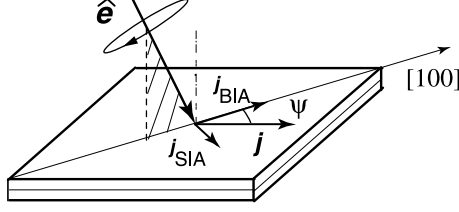


Figure 4: SIA and BIA- induced circular photogalvanic effect generated in samples of C_{2v} symmetry under oblique incidence of circularly polarized light with excitation along $[110]$.

current \mathbf{j} is perpendicular to the direction of light propagation $\hat{\mathbf{e}}$. If the radiation is shined in along a cubic axis $\langle 100 \rangle$, with $\hat{e}_x = \hat{e}_y = 1/\sqrt{2}$, then the current is longitudinal flowing along the same cubic axis because $j_x = j_y$. Putting all together, we see from Eqs. (13) that rotating $\hat{\mathbf{e}}$ in the plane of the QW counter-clockwise yields a clockwise rotation of \mathbf{j} .

Reducing the symmetry from D_{2d} to C_{2v} , the tensor γ describing the CPGE is characterized by two independent components γ_{xy} and $\gamma_{yx} \neq \gamma_{xy}$. We define $\gamma^{(1)} = \gamma_{xy}$ and $\gamma^{(2)} = \gamma_{yx}$, then the photocurrent is determined by

$$j_x = \gamma^{(1)} \hat{e}_y E_0^2 P_{\text{circ}}, \quad j_y = \gamma^{(2)} \hat{e}_x E_0^2 P_{\text{circ}}. \quad (14)$$

If $\hat{\mathbf{e}}$ is along $\langle 110 \rangle$ so as $\hat{e}_x = 1$ and $\hat{e}_y = 0$ or $\hat{e}_x = 0$ and $\hat{e}_y = 1$, then the current again flows normal to the light propagation direction. In contrast to D_{2d} symmetry the strength of the current is different for the radiation propagating along x or y . This is due to the non-equivalence of the crystallographic axes $[1\bar{1}0]$ and $[110]$ because of the two-fold rotation axis in C_{2v} symmetry. If the sample is irradiated with $\hat{\mathbf{e}}$ parallel to $\langle 100 \rangle$ corresponding to $\hat{e}_x = \hat{e}_y = 1/\sqrt{2}$, the current is neither parallel nor perpendicular to the light propagation direction (see Fig. 4). The current includes an angle ψ with the x -axis given by $\tan \psi = \gamma_{xy}/\gamma_{yx} = \beta_{yx}/\beta_{xy}$. The last equation follows from tensor equivalence.

Another conclusion from Eqs. (13) and (14) is that in QWs of the higher symmetries D_{2d} and C_{2v} the photocurrent can only be induced under oblique incidence of irradiation. For normal incidence $\hat{\mathbf{e}}$ is parallel to $[001]$ and hence the current vanishes as $\hat{e}_x = \hat{e}_y = 0$. In contrast to this result in QWs of C_s symmetry a photocurrent also occurs for normal incidence of the radiation on the plane of the QW because the tensor γ has an additional component $\gamma_{xz'}$. The current here is given by

$$j_x = (\gamma_{xy'} \hat{e}_{y'} + \gamma_{xz'} \hat{e}_{z'}) E_0^2 P_{\text{circ}}, \quad j_{y'} = \gamma_{y'x} \hat{e}_x E_0^2 P_{\text{circ}}. \quad (15)$$

At normal incidence, $\hat{e}_x = \hat{e}_{y'} = 0$ and $\hat{e}_{z'} = 1$, the current in the QW flows perpendicular to the mirror reflection plane of C_s which corresponds to the x coordinate parallel to $[1\bar{1}0]$.

Now we will take a closer look on the dependence of the photocurrent on the angle of incidence Θ_0 which is determined by the value of the projection $\hat{\mathbf{e}}$ on the x - (y -) axis (see Eqs. (13) and (14)) or on the z' -axis (Eqs. (15)). We have for the excitation in the plane of incidence parallel to (yz)

$$\hat{e}_x = t_p t_s \sin \Theta, \quad (16)$$

and in the plane of incidence parallel to $(y'z')$

$$\hat{e}_{z'} = t_p t_s \cos \Theta, \quad (17)$$

where Θ is the refraction angle defined by $\sin \Theta = \sin \Theta_0 / \sqrt{\epsilon^*}$, ϵ^* is the dielectric constant of the QW material, and transmission coefficients t_p , t_s for linear p and s polarizations after Fresnel's formula are given by

$$t_p t_s = \frac{4 \cos^2 \Theta_0}{\left(\cos \Theta_0 + \sqrt{\epsilon^* - \sin^2 \Theta_0} \right) \left(\epsilon^* \cos \Theta_0 + \sqrt{\epsilon^* - \sin^2 \Theta_0} \right)}. \quad (18)$$

For $\hat{e}_{y'}$ in the left equation of Eqs. (15) we obtain $\hat{e}_{y'} = t_p t_s \sin \Theta$ for the excitation in the plane of incidence parallel to $(y'z)$.

The measurement of the CPGE with respect to the angle of incidence and the crystallographic direction is important to determine the in-plane symmetry of the QW. Indeed, only in C_s symmetry CPGE occurs at normal incidence (see Eqs. (15)), and D_{2d} and C_{2v} symmetries may be distinguished by excitation along a $\langle 100 \rangle$ axis, because in this case only D_{2d} does not allow a transverse effect.

2.2.3 Microscopic theory

Inter-band transitions: The microscopic theory of spin orientation induced CPGE in QWs was worked out for inter-band excitation in [21, 25, 26] and is briefly sketched here following [21]. We consider the asymmetry of the momentum distribution of holes excited under direct inter-band optical transitions in p -doped (113)-grown QWs of C_s symmetry. We remind that in this case normal incident radiation of circular polarization induces a current in x direction. Let us denote the free hole states in a QW as $|\nu m_s \mathbf{k}\rangle$, where ν and m_s are the hole subband and spin-branch indices, respectively. If only terms even in \mathbf{k} are taken into account in the effective Hamiltonian of holes, all hole subbands (ν, \mathbf{k}) are doubly degenerate. Allowing terms odd in \mathbf{k} in the Hamiltonian results in a subband spin splitting so that the hole energy $\varepsilon_{\nu m_s \mathbf{k}}$ becomes dependent on the spin branch index m_s . The photocurrent density is given by a standard expression

$$j_x = e \sum_{\nu m_s \mathbf{k}} u_x(\nu m_s \mathbf{k}) f_{\nu m_s \mathbf{k}}, \quad (19)$$

where e is the elementary charge (for holes $e > 0$), $u_x(\nu m_s \mathbf{k})$ is the group velocity $\hbar^{-1}(\partial \varepsilon_{\nu m_s \mathbf{k}} / \partial k_x)$ and $f_{\nu m_s \mathbf{k}}$ is the non-equilibrium steady-state distribution function. Note that the energy $\varepsilon_{\nu m_s \mathbf{k}}$ is invariant and the velocity $u_x(\nu m_s \mathbf{k})$ changes its sign under the time-inversion operation K transforming a spinor $\hat{\psi}$ into $K\hat{\psi} \equiv i\sigma_y \hat{\psi}$ (σ_y is one of the Pauli matrices) [14]. Therefore only the anti-symmetric part of the distribution function $f_{\nu m_s \mathbf{k}}^- = (f_{\nu m_s \mathbf{k}} - f_{\nu \bar{m}_s, -\mathbf{k}})/2$ contributes to j_x . Here $|\nu \bar{m}_s, -\mathbf{k}\rangle$ is obtained from $|\nu m_s \mathbf{k}\rangle$ by application of the operator K .

In the momentum relaxation time approximation under direct optical transitions we have

$$j_x = e \sum_{\nu' \nu m'_s m_s \mathbf{k}} W_{\nu' m'_s, \nu m_s}(\mathbf{k}, \mathbf{e}) \left[u_x(\nu' m'_s \mathbf{k}) \tau_p^{(\nu')} - u_x(\nu m_s \mathbf{k}) \tau_p^{(\nu)} \right], \quad (20)$$

where \mathbf{e} is the light polarization unit vector and $\tau_p^{(\nu)}$ is the hole momentum relaxation time in the subband ν . The probability rate for the transition $|\nu m_s \mathbf{k}\rangle \rightarrow |\nu' m'_s \mathbf{k}\rangle$ is given by Fermi's golden rule

$$W_{\nu' m'_s, \nu m_s}(\mathbf{k}, \mathbf{e}) = \frac{2\pi}{\hbar} |M_{\nu' m'_s, \nu m_s}(\mathbf{k})|^2 (f_{\nu m_s \mathbf{k}}^0 - f_{\nu' m'_s \mathbf{k}}^0) \delta(\varepsilon_{\nu' m'_s \mathbf{k}} - \varepsilon_{\nu m_s \mathbf{k}} - \hbar\omega), \quad (21)$$

where $M_{\nu' m'_s, \nu m_s}(\mathbf{k})$ is the inter-subband optical matrix element proportional to the amplitude of the electromagnetic field E_0 and $f_{\nu m_s \mathbf{k}}^0$ is the distribution function in equilibrium. For the sake of simplicity, it is assumed that the light intensity is low enough to ignore a photoinduced redistribution of the symmetrical part $f_{\nu m_s \mathbf{k}}^+ = (f_{\nu m_s \mathbf{k}} + f_{\nu \bar{m}_s, -\mathbf{k}})/2$.

The most important result of the microscopic theory is that both the initial and final states of the carriers involved in the optical transition contribute to the circular photogalvanic current with different strength and directions. The partial currents are proportional to the group velocity being dependent on \mathbf{k} , the momentum relaxation time τ_p , and the occupation of the initial states described by the distribution function. Therefore the direction of total current depends of the details of experimental conditions and may change its sign by varying the radiation frequency, temperature etc. An interesting feature of spin orientation induced CPGE at inter-band excitation was pointed out in [25, 26] showing that varying the frequency around the fundamental band edge results in sign inversion of the current due to SIA contribution but not to BIA.

Inter-subband transitions: The microscopic theory of spin orientation induced CPGE was also developed for direct inter-subband transitions in n -type QWs for both C_s and C_{2v} symmetry with the result that the current is proportional to the derivative of the absorbance [24]. For the typical condition of inter-subband transitions in n -type QWs that the momentum relaxation time

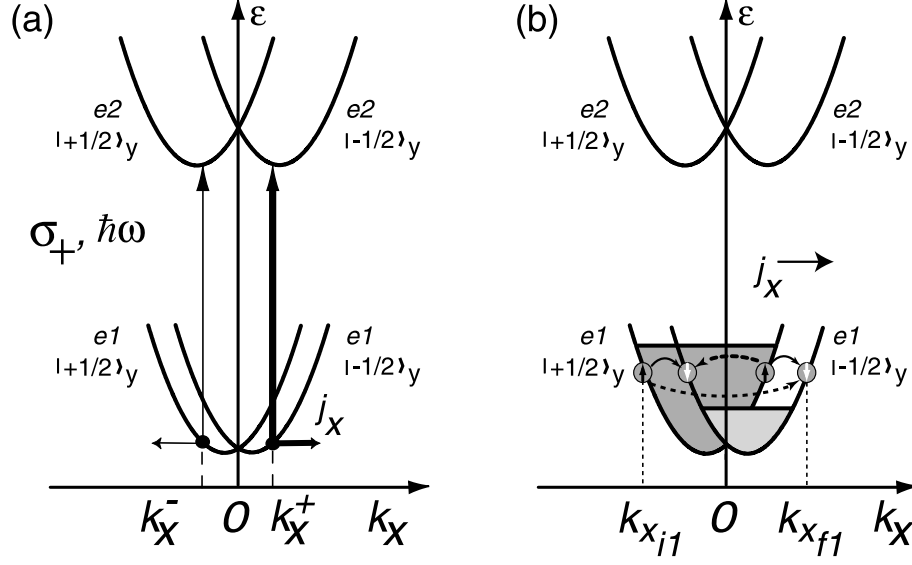


Figure 5: Microscopic picture of (a) circular photogalvanic effect and (b) spin-galvanic effect at inter-subband excitation in C_{2v} point group samples. In (a) the current j_x is caused by the imbalance of optical transition probabilities at k_x^- and k_x^+ decaying with the momentum relaxation time τ_p . Excitation with σ_+ radiation of $\hbar\omega$ less than the energy subband separation at $\mathbf{k}=0$, ε_{21} , induces direct spin-conserving transitions (vertical arrows) at k_x^- and k_x^+ . The rates of these transitions are different as illustrated by the different thickness of the arrows (reversing the angle of incidence mirrors the thicknesses of arrows). This leads to a photocurrent due to an asymmetrical distribution of carriers in \mathbf{k} -space if the splitting of the $e1$ and $e2$ subbands is non-equal. Increasing of the photon energy shifts more intensive transitions to the left and less intensive to the right resulting in a current sign change. In (b) the current occurs after thermalization in the lowest subband which results in the spin orientation in $e1$ subband. This spin-galvanic current is caused by asymmetric spin-flip scattering. The rate of spin-flip scattering depends on the value of the initial and final \mathbf{k} -vectors. Thus transitions sketched by dashed arrows yield an asymmetric occupation of both subbands and hence a current flow which decays with the spin relaxation time τ_s . The magnitude of the spin polarization and hence the current depends on the initial absorption strength but not on the momentum \mathbf{k} of transition. Therefore the shape of the spectrum of the spin-galvanic current follows the absorption.

of photoexcited carriers in the $e2$ subband, $\tau_p^{(2)}$, is much less than that in the $e1$ subbands, $\tau_p^{(1)}$, it was obtained that for C_s symmetry

$$j_x \sim \left(\beta_{yx}^{(2)} + \beta_{yx}^{(1)} \right) \frac{d\eta_{12}(\hbar\omega)}{d\hbar\omega} \tau_p^{(1)} I P_{circ} \hat{e}_y, \quad (22)$$

where η_{12} is the absorbance, I is the radiation intensity, $\beta_{yx}^{(1)}$ and $\beta_{yx}^{(2)}$ are components of β in the $e1$ and $e2$ subbands, respectively. The analogue equation was obtained also for QWs of C_{2v} symmetry. In contrast to spin-flip processes occurring for C_s symmetry described above in C_{2v} symmetry due to selection rules the absorption of circularly polarized radiation is spin-conserving [14]. The asymmetric distribution of photo-excited electrons resulting in a current is caused by these spin-conserving but spin-dependent transitions. It was shown in [24, 91] that under oblique excitation by circularly polarized light the rates of inter-subband transitions are different for electrons with the spin oriented co-parallel and anti-parallel to the in-plane direction of light propagation. This is depicted in Fig. 5a by vertical arrows of different thicknesses. In systems with \mathbf{k} -linear spin splitting such processes lead to an asymmetrical distribution of carriers in \mathbf{k} -space, i.e. to an electrical current. Also for these symmetry the photocurrent is proportional to the derivative of absorption and is given by

$$j_x \sim \left(\beta_{yx}^{(2)} - \beta_{yx}^{(1)} \right) \frac{d\eta_{12}(\hbar\omega)}{d\hbar\omega} \tau_p^{(1)} I P_{circ} \hat{e}_y. \quad (23)$$

Since the circular photogalvanic effect in QW structures of C_{2v} symmetry is caused by spin-dependent *spin-conserving* optical transitions, the photocurrent described by Eq. (23) in contrast to Eq. (22) is proportional to the difference of subband spin splittings.

2.2.4 One- and two-photon excitation

One more spin photocurrent related to the photogalvanic effect was proposed in [32] and has most recently been observed in bulk GaAs [33]. The generation of the photocurrent is based on quantum interference of one- and two-photon excitation [92] which represents a coherent photogalvanic effect [34]. Irradiation of a semiconductor sample with a coherent superposition of laser beam of frequency ω satisfying $E_g/2 < \hbar\omega < E_g$ and its second harmonic may yield an electric current if there are definite phase relations of the radiation fields. Tuning of the phase relation among the coherent beams allows a control of the current. In order to obtain a spin photocurrent proper polarization of both beams is required. If the radiation fields at ω and 2ω have either the same circular polarization or orthogonal linear polarizations, quantum interference at injection distinguishes carriers of opposite spin which results in a net spin flux. It is possible to obtain spin photocurrent without electric current flow. The asymmetry of spin population in \mathbf{k} -space appears as a consequence of spin-orbit coupling. The photocurrent is mediated by a fourth rank tensor and thus needs no symmetry restriction as in the case of one-photon excitation photogalvanic effect. It may be present in materials with a center of inversion. So far coherent control of a spin photocurrent has been observed in bulk semiconductors (GaAs) [33] but it may also be possible in QWs and in asymmetric superlattices [35].

2.3 Spin-galvanic effect

The picture of spin photocurrents given so far involved the asymmetry of the momentum distribution of photoexcited carriers, i.e. the spin orientation induced CPGE. In addition to CPGE a spin driven current may also occur even after momentum relaxation of photoexcited carriers. It is due to an asymmetry of spin-flip scattering of non-equilibrium spin polarized carriers as shown in Fig. 5b. This current is caused by the spin-galvanic effect and will be described in the following.

2.3.1 Phenomenology

The spin-galvanic effect is caused by spin relaxation of a uniform non-equilibrium spin polarization in QWs of gyrotropic symmetry [29]. While this effect may occur at any method of spin orientation e.g. electric spin injection, optical spin polarization is also possible resulting in a spin photocurrent. Phenomenologically, an electric current can be linked to the electron's averaged spin polarization \mathbf{S} by

$$j_\alpha = \sum_{\gamma} Q_{\alpha\gamma} S_\gamma. \quad (24)$$

Like in the case of \mathbf{k} -linear terms and CPGE here we have again a second rank pseudo-tensor \mathbf{Q} with the same symmetry restrictions like β and γ . Therefore in zinc-blende structure QW, non-zero components of $Q_{\alpha\gamma}$ exist in contrast to the corresponding bulk crystals [27, 28]. Due to tensor equivalence we have the same non-zero components of the tensor \mathbf{Q} and their relations as discussed above for β and γ . For C_{2v} symmetry of (001)-grown QWs only two linearly independent components, Q_{xy} and Q_{yx} , may be non-zero so that

$$j_x = Q_{xy} S_y, \quad j_y = Q_{yx} S_x. \quad (25)$$

Hence, a spin polarization driven current needs a spin component lying in the plane of QWs. In D_{2d} symmetry there is only one independent tensor component $Q_{xy} = Q_{yx}$. In C_s symmetry of (113)-oriented QWs an additional tensor component $Q_{xz'}$ may be non-zero and the spin-galvanic current may be driven by spins oriented normally to the plane of QW.

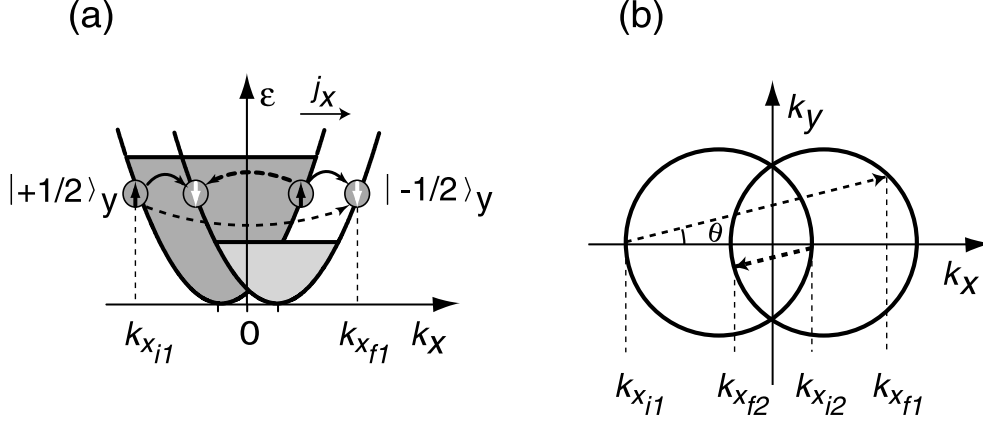


Figure 6: Microscopic origin of the spin-galvanic current in the presence of \mathbf{k} -linear terms in the electron Hamiltonian. (a) one-dimensional sketch: the $\sigma_y k_x$ term in the Hamiltonian splits the conduction band into two parabolas with the spin $m_s = \pm 1/2$ in the y -direction. If one spin subband is preferentially occupied, e.g., by spin injection (the $|+1/2\rangle_y$ -states in the figure) asymmetric spin-flip scattering results in a current in x -direction. The rate of spin-flip scattering depends on the value of the initial and final \mathbf{k} -vectors. Thus transitions sketched by dashed arrows yield an asymmetric occupation of both subbands and hence a current flow. These transitions are also shown in two dimensions (b) by dashed arrows at scattering angle θ . If instead of the spin-down subband the spin-up subband is preferentially occupied the current direction is reversed.

2.3.2 Microscopic model

Microscopically, the spin-galvanic effect is caused by asymmetric spin-flip relaxation of spin polarized electrons in systems with \mathbf{k} -linear contributions to the effective Hamiltonian [29]. Fig. 6a sketches the electron energy spectrum along k_x with the spin dependent term $\beta_{yx}\sigma_y k_x$ resulting from BIA and SIA. In this case σ_y is a good quantum number. Spin orientation in y -direction causes the unbalanced population in spin-down and spin-up subbands. The current flow is caused by \mathbf{k} -dependent spin-flip relaxation processes. Spins oriented in y -direction are scattered along k_x from the higher filled, e.g. spin subband $|+1/2\rangle_y$ to the less filled spin subband $|-1/2\rangle_y$. Four quantitatively different spin-flip scattering events exist and are sketched in Fig. 6a by bent arrows. The spin-flip scattering rate depends on the values of the wavevectors of the initial and the final states [47]. Therefore spin-flip transitions, shown by solid arrows in Fig. 6a, have the same rates. They preserve the symmetric distribution of carriers in the subbands and, thus, do not yield a current. However, the two scattering processes shown by broken arrows are inequivalent and generate an asymmetric carrier distribution around the subband minima in both subbands. This asymmetric population results in a current flow along the x -direction. Within this model of elastic scattering the current is not spin polarized since the same number of spin-up and spin-down electrons move in the same direction with the same velocity.

It must be pointed out that the above one-dimensional model, which in a clear way demonstrates how a spin-galvanic current can occur, somehow simplifies the microscopic picture. The probability of the spin-flip processes $|+1/2, \mathbf{k}_i\rangle_y \rightarrow |-1/2, \mathbf{k}_f\rangle_y$ shown by arrows in Fig. 6 is given by the product $[v(\mathbf{k}_i - \mathbf{k}_f)]^2 (\mathbf{k}_f + \mathbf{k}_i)^2$ (see Eq. (30) of [47]). The amplitude $v(\mathbf{k}_f - \mathbf{k}_i)$ depends on $\mathbf{k}_f - \mathbf{k}_i$ and therefore the spin-flip process is asymmetric as needed for the occurrence of the current. However, for the one-dimensional model presented above the probability is given by $[v(k_{xf} - k_{xi})]^2 (k_{xf} + k_{xi})^2$. In the case of elastic scattering, as sketched in Fig. 6a, the magnitudes of the initial and final wavevectors are equal, $|k_{xi}| = |k_{xf}|$, thus $k_{xf} + k_{xi} = 0$ and the probability vanishes. A non-zero current is obtained at inelastic scattering and at elastic scattering with $k_y \neq 0$. The latter situation is depicted in Fig. 6b.

Note that the reverse process to the spin-galvanic effect i.e. a spin polarization induced by an electric current flow has been theoretically considered in [93, 94].

The uniformity of spin polarization in space is preserved during the scattering processes. Therefore the spin-galvanic effect differs from other experiments where the spin current is caused by

inhomogeneities. These effects will be discussed in section 6.

2.3.3 Microscopic theory

The microscopic theory of the spin-galvanic effect has been developed in [31] for inter-subband transitions in n -type zinc-blende structure materials of C_{2v} symmetry. In this case the spin orientation (see Fig. 5b) is generated by resonant spin-selective optical excitation (see Fig. 5a) followed by spin-non-specific thermalization.

The occurrence of a current is due to the spin dependence of the electron scattering matrix elements $M_{\mathbf{k}'\mathbf{k}}$. The 2×2 matrix $\hat{M}_{\mathbf{k}'\mathbf{k}}$ can be written as a linear combination of the unit matrix \hat{I} and Pauli matrices as follows

$$\hat{M}_{\mathbf{k}'\mathbf{k}} = A_{\mathbf{k}'\mathbf{k}}\hat{I} + \boldsymbol{\sigma} \cdot \mathbf{B}_{\mathbf{k}'\mathbf{k}}, \quad (26)$$

where $A_{\mathbf{k}'\mathbf{k}}^* = A_{\mathbf{k}\mathbf{k}'}$, $B_{\mathbf{k}'\mathbf{k}}^* = B_{\mathbf{k}\mathbf{k}'}$ due to hermiticity of the interaction and $A_{-\mathbf{k}',-\mathbf{k}} = A_{\mathbf{k}\mathbf{k}'}$, $B_{-\mathbf{k}',-\mathbf{k}} = -B_{\mathbf{k}\mathbf{k}'}$ due to the symmetry under time inversion. The spin-dependent part of the scattering amplitude in (001)-grown QW structures is given by [47]

$$\boldsymbol{\sigma} \cdot \mathbf{B}_{\mathbf{k}'\mathbf{k}} = v(\mathbf{k} - \mathbf{k}')[\sigma_x(k'_y + k_y) - \sigma_y(k'_x + k_x)]. \quad (27)$$

We note that Eq. (27) determines the spin relaxation time, τ'_s , due to the Elliot-Yafet mechanism. The spin-galvanic current, for instance in y direction, has the form [31]

$$j_{SGE,x} = Q_{xy}S_y \sim e n_e \frac{\beta_{yx}^{(1)}}{\hbar} \frac{\tau_p}{\tau'_s} S_y, \quad j_{SGE,y} = Q_{yx}S_x \sim e n_e \frac{\beta_{xy}^{(1)}}{\hbar} \frac{\tau_p}{\tau'_s} S_x. \quad (28)$$

Since scattering is the origin of the spin-galvanic effect, the spin-galvanic current, j_{SGE} , is determined by the Elliot-Yafet spin relaxation time. The relaxation time τ'_s is proportional to the momentum relaxation time τ_p . Therefore the ratio τ_p/τ'_s in Eqs. (28) does not depend on the momentum relaxation time. The in-plane average spin S_x in Eqs. (28) decays with the total spin relaxation time τ_s (which may have a contribution from any spin relaxing process). Thus the time decay of the spin-galvanic current following a pulsed photoexcitation is determined by τ_s .

For the case, where spin relaxation is obtained as a result of inter-subband absorption of circularly polarized radiation, the current is given by

$$j_{SGE,x} = Q_{xy}S_y \sim e \frac{\beta_{yx}^{(1)}}{\hbar} \frac{\tau_p \tau_s}{\tau'_s} \frac{\eta_{21} I}{\hbar \omega} P_{circ} \xi \hat{e}_y, \quad j_{SGE,y} = Q_{yx}S_x \sim e \frac{\beta_{xy}^{(1)}}{\hbar} \frac{\tau_p \tau_s}{\tau'_s} \frac{\eta_{21} I}{\hbar \omega} P_{circ} \xi \hat{e}_x. \quad (29)$$

where η_{21} is the absorbance at the transitions between $e1$ and $e2$ subbands. The parameter ξ , varying between 0 and 1, is the ratio of photoexcited electrons relaxing to the $e1$ subband with and without spin-flip. It determines the degree of spin polarization in the lowest subband (see Fig. 4b) and depends on the details of the relaxation mechanism. Optical orientation requires $\xi \neq 0$ [3, 91, 95]. Eqs. (29) show that the spin-galvanic current is proportional to the absorbance and is determined by the spin splitting in the first subband, $\beta_{yx}^{(1)}$ or $\beta_{xy}^{(1)}$.

2.3.4 Spin-galvanic effect at optical orientation

Excitation of QWs by circularly polarized light results in a spin polarization which, at proper orientation of the electron spins, causes a photocurrent due to the spin-galvanic effect. Because of the tensor equivalence the spin-galvanic current induced by circularly polarized light always occurs simultaneously with the spin orientation induced CPGE. The two effects can be separated by time-resolved measurements because of the different relaxation mechanisms of the two currents. After removal of light or under pulsed photoexcitation the circular photogalvanic current decays with the momentum relaxation time whereas the spin-galvanic current decays with the spin relaxation time. On the other hand, as it has been recently shown [31], at inter-subband transitions the spin-galvanic effect may be separated from CPGE making use of the spectral behaviour at resonance. The optically induced spin-galvanic current reproduces the absorbance whereas CPGE is proportional to the derivative of the absorbance and vanishes at the resonance frequency. This will be discussed in more detail in section 4.2.2.

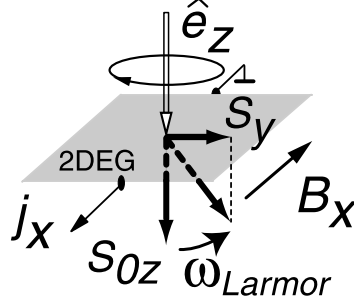


Figure 7: Optical scheme of generating a uniform in-plane spin-polarization which causes spin-galvanic photocurrent. Electron spins are oriented normal to the plane of QW by circularly polarized radiation and rotated into the plane by Larmor precession in a magnetic field B_x .

2.3.5 Spin-galvanic effect at optical orientation in the presence of magnetic field

Another possibility to investigate the spin-galvanic effect without contributions of the spin orientation induced CPGE to the current has been introduced in [29]. This method is not limited to resonant inter-subband optical excitation. The spin polarization was obtained by absorption of circularly polarized radiation at normal incidence on (001)-grown QWs as depicted in Fig. 7. For normal incidence the spin orientation induced CPGE as well as the spin-galvanic effect vanish because $\hat{e}_x = \hat{e}_y = 0$ (see Eqs. (14)) and $S_x = S_y = 0$ (see Eqs.(25)), respectively. Thus, we obtain a spin orientation along the z coordinate but no spin photocurrent.

The steady-state spin polarization S_{0z} is proportional to the spin generation rate \dot{S}_z . To obtain an in-plane component of the spins, necessary for the spin-galvanic effect, a magnetic field $\mathbf{B} \parallel x$ has been applied. Due to Larmor precession a non-equilibrium spin polarization S_y is induced being

$$S_y = -\frac{\omega_L \tau_{s\perp}}{1 + (\omega_L \tau_s)^2} S_{0z}, \quad (30)$$

where $\tau_s = \sqrt{\tau_{s\parallel} \tau_{s\perp}}$, $\tau_{s\parallel}$, $\tau_{s\perp}$ are the longitudinal and transverse electron spin relaxation times, ω_L is the Larmor frequency. The denominator in Eq. (30) yielding the decay of S_y for ω_L exceeding the inverse spin relaxation time is well known from the Hanle effect [3, 96]

On a phenomenological level and at small magnetic fields, $\omega_L \tau_s \ll 1$, this magnetic field induced spin photocurrent can be described by

$$j_\alpha = \sum_{\beta\gamma} \mu_{\alpha\beta\gamma} B_\beta i(E \times E^*)_\gamma = \sum_{\beta\gamma} \mu_{\alpha\beta\gamma} B_\beta \hat{e}_\gamma E_0^2 P_{circ}, \quad (31)$$

where $\mu_{\alpha\beta\gamma}$ is a third rank tensor. As P_{circ} is a pseudo-scalar and \mathbf{B} a pseudo-vector, $\mu_{\alpha\beta\gamma}$ is a regular negative-parity third rank tensor which is allowed in inversion asymmetric materials only. Gyrotropy at zero magnetic field, as in the case of only optical excited spin-galvanic effect or of circular photogalvanic effect, is not necessary. We note that in non-gyrotropic p -type bulk GaAs a magnetic field induced circular photogalvanic effect was previously observed at intra-band excitation [97]. However, this effect is not due to spin orientation and does not occur in p -type QWs due to spatial quantization [98]. In QWs under normal incidence of the light and for a magnetic field lying in the plane of a QW of C_{2v} symmetry, which corresponds to the measurements in section 4.2.1 the current is described by two independent components of the tensor $\boldsymbol{\mu}$ and can be written as

$$j_x = \mu_{xxz} B_x \hat{e}_z E_0^2 P_{circ}, \quad j_y = \mu_{yyz} B_y \hat{e}_z E_0^2 P_{circ}. \quad (32)$$

The current \mathbf{j} and the magnetic field \mathbf{B} are parallel (or anti-parallel) when the magnetic field is applied along $\langle 110 \rangle$ and neither parallel nor perpendicular for $\mathbf{B} \parallel \langle 100 \rangle$. In D_{2d} -symmetry QWs with symmetric interfaces $\mu_{xxz} = -\mu_{yyz}$ and therefore the current is perpendicular to the magnetic field for $\mathbf{B} \parallel \langle 100 \rangle$.

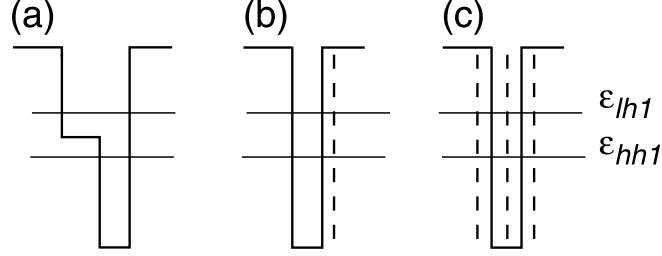


Figure 8: Potential profiles of SiGe QW samples: (a) compositionally stepped QW, (b) asymmetrically doped compositionally symmetric QW, and (c) symmetric QW. The vertical dashed lines indicate the doping.

2.4 Spin orientation induced circular photogalvanic effect versus spin-galvanic effect

The spin orientation induced circular photogalvanic effect and the spin-galvanic effect have in common that the current flow is driven by an asymmetric distribution of carriers in \mathbf{k} -space in systems with lifted spin degeneracy due to \mathbf{k} -linear terms in the Hamiltonian. The crucial difference between both effects is, that the spin-galvanic effect may be caused by any means of spin injection, while the spin orientation induced CPGE needs optical excitation with circularly polarized radiation. Even if the spin-galvanic effect is achieved by optical spin orientation, as discussed here, the microscopic mechanisms are different. The spin-galvanic effect is caused by asymmetric spin-flip scattering of spin polarized carriers and it is determined by the process of spin relaxation (see Fig. 6). If spin relaxation is absent, the spin-galvanic current vanishes. In contrast, the spin orientation induced CPGE is the result of selective photoexcitation of carriers in \mathbf{k} -space with circularly polarized light due to optical selection rules and depends on momentum relaxation (see Fig. 2). In some optical experiments the observed photocurrent may represent a sum of both effects. For example, if we irradiate an (001)-oriented QW at oblique incidence of circularly polarized radiation, we obtain both, selective photoexcitation of carriers in \mathbf{k} -space determined by momentum relaxation and spin-galvanic effect due to an in-plane component of non-equilibrium spin polarization. Thus both effects contribute to the current occurring in the plane of the QW. The two mechanisms can be distinguished by time resolved measurements.

3 Methods

3.1 Samples

The experiments were carried out on GaAs, InAs, semimagnetic BeZnMnSe and SiGe heterostructures belonging to two different classes of symmetry. Higher symmetric structures were (001)-oriented QWs. While these structures can belong to two point groups, either D_{2d} or C_{2v} our measurements showed that all samples available for the present work correspond to the point group C_{2v} . Structures of the lower symmetry class C_s were (113)-oriented QWs and quantum wells grown on (001)-misut substrates.

Zinc-blende structure based QW samples were molecular-beam-epitaxy (MBE) grown n - and p -type GaAs/AlGaAs with QW widths L_W of 4 nm to 20 nm [20,24,38], n -type InAs/AlGaSb QWs with $L_W=15$ nm [20,99] as well as single n -type GaAs heterojunctions. Free carrier densities, n_s for electrons and p_s for holes, ranged from 10^{11} cm^{-2} to $2 \cdot 10^{12} \text{ cm}^{-2}$. The mobility at 4.2 K in n -type samples was from $5 \cdot 10^5 \text{ cm}^2/\text{Vs}$ to $2 \cdot 10^6 \text{ cm}^2/\text{Vs}$ and in p -type samples was about $5 \cdot 10^5 \text{ cm}^2/\text{Vs}$.

Semimagnetic BeZnMnSe semiconductor heterostructures were grown by MBE on semi-insulating GaAs substrates with (001) orientation [43,100]. The heterostructures consisted of a 500-nm-thick $\text{Be}_{0.03}\text{Zn}_{0.97}\text{Se}$ layer n -doped to $2 \cdot 10^{18} \text{ cm}^{-3}$ followed by an 100 nm thick $\text{Be}_{0.05}\text{Zn}_{0.89}\text{Mn}_{0.06}\text{Se}$ layer n -doped to $6 \cdot 10^{18} \text{ cm}^{-3}$.

The measurements on SiGe QWs were carried out on p -type structures MBE-grown on (001)- and (113)-oriented Si substrates [23]. Both bulk Si as well as Ge have a center of inversion, therefore

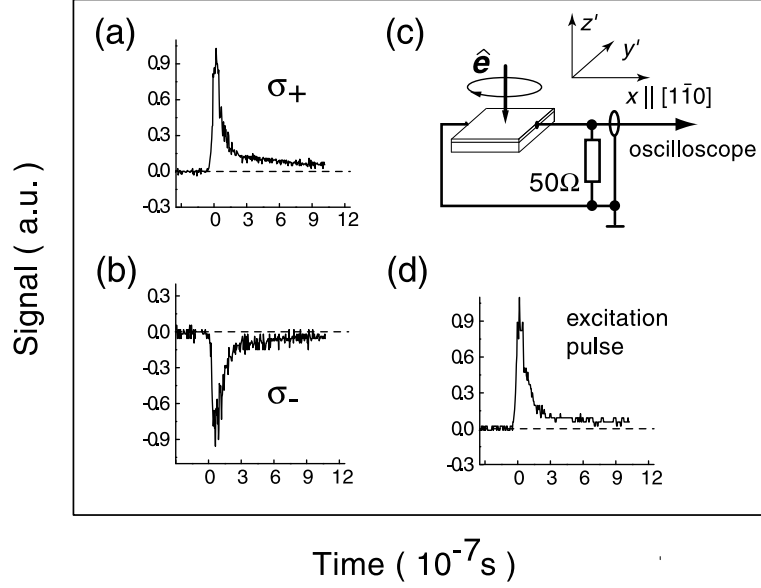


Figure 9: Oscilloscope traces obtained for pulsed excitation of (113)-grown *n*-type GaAs QWs at $\lambda = 10.6 \mu\text{m}$. (a) and (b) show CPGE signals obtained for σ_+ and σ_- -circular polarization, respectively. For comparison in (d) a signal pulse of a fast photon drag detector is plotted. In (c) the measurement arrangement is sketched. For (113)-grown samples being of C_s symmetry radiation was applied at normal incidence and the current detected in the direction $x \parallel [1\bar{1}0]$. For (001)-grown QWs oblique incidence was used in order to obtain the helicity dependent current.

in order to obtain gyrotropy asymmetric QWs were grown. Two groups of (001)-grown asymmetric samples, whose potential profiles are sketched in Figs. 8a and 8b, were fabricated in the following manner: one of the groups of samples was compositionally stepped (Fig. 8a) comprising 10 QWs $[\text{Si}_{0.75}\text{Ge}_{0.25}(4 \text{ nm})/\text{Si}_{0.55}\text{Ge}_{0.45}(2.4 \text{ nm})]$ separated by 6 nm Si barriers. The second group of asymmetric structures had a single QW of $\text{Si}_{0.75}\text{Ge}_{0.25}$ composition which was doped with boron from one side only (Fig. 8b). These structures are of the C_{2v} point group symmetry which was confirmed by the experiments described below. Structures of the lower symmetry C_s were (113)-grown with a $\text{Si}/\text{Si}_{0.75}\text{Ge}_{0.25}(5 \text{ nm})/\text{Si}$ single QW one-side boron doped. As a reference sample a (001)-grown compositionally symmetric and symmetrically boron doped multiple QW structure (Fig. 8c) of sixty $\text{Si}_{0.7}\text{Ge}_{0.3}(3 \text{ nm})$ QW has been used. All these samples had free carrier densities p_s of about $8 \cdot 10^{11} \text{ cm}^{-2}$ in each QW.

The sample edges were oriented along the $[1\bar{1}0]$ - and $[33\bar{2}]$ - directions for the (113)-grown sample and along the $[1\bar{1}0]$ - and $[110]$ - directions for the (001)-grown. For (113)-oriented samples two pairs of ohmic contacts were centered along opposite sample edges pointing in the directions $x \parallel [1\bar{1}0]$ and $y \parallel [33\bar{2}]$ (see Fig. 9 and inset in Fig. 10, lower plate). For (001)-oriented samples two pairs of point contacts in the middle of the sample edges with connecting lines along $x \parallel [1\bar{1}0]$ and $y' \parallel [110]$ were prepared (see inset in Fig. 10, upper plate). These samples had two additional pairs of contacts at the corners of the samples corresponding to the $\langle 100 \rangle$ -directions (see inset in Fig. 10, upper plate).

3.2 Experimental technique

For optical excitation mid-infrared (MIR), far-infrared (FIR) and visible laser radiation was used. Most of the measurements were carried out in the infrared with photon energies less than the energy gap of investigated semiconductors. For investigations of spin photocurrents infrared excitation has several advantages. First of all below the energy gap the absorption is very weak and therefore allows homogeneous excitation with marginal heating of the 2D electron gas. Furthermore, in contrast to inter-band excitation, there are no spurious photocurrents due to other mechanisms like the Dember effect, photovoltaic effects at contacts and Schottky barriers etc. Depending on the photon energy and QW band structure the MIR and FIR radiation induce direct optical transitions

between size quantized subbands in n - and p -type samples or, at longer wavelength, indirect optical transitions (Drude absorption) in the lowest subband.

A high power pulsed mid-infrared (MIR) transversely excited atmospheric pressure carbondioxide (TEA-CO₂) laser and a molecular far-infrared (FIR) laser [101,102] have been used as radiation sources in the spectral range between 9.2 μm and 496 μm . The corresponding photon energies $\hbar\omega$ lie in the range of 135 meV to 2 meV. The radiation pulses ($\simeq 100$ ns) of a power P up to 50 kW were focused to a spot of about 1 mm² yielding a maximum intensity of about 5 MW/cm². Such high intensities are only needed for saturation measurements describes in section 4.4. The power required to detect spin photocurrents is much lower. One series of measurements was carried out making use of the frequency tunability of the free electron laser "FELIX" at FOM-Rijnhuizen in The Netherlands [103]. The FELIX operated in the spectral range between 7 μm and 12 μm . The output pulses of light from FELIX were chosen to be 3 ps long, separated by 40 ns, in a train (or "macropulse") of 5 μs duration. The macropulses had a repetition rate of 5 Hz.

Typically these lasers emit linearly polarized radiation. The polarization was modified from linear to circular using a Fresnel rhomb and $\lambda/4$ plates for MIR and FIR radiation, respectively. The helicity P_{circ} of the incident light was varied from -1 (left-handed circular, σ_-) to $+1$ (right-handed circular, σ_+) according to $P_{\text{circ}} = \sin 2\varphi$ (see Eq. (12)). In the present experimental arrangement the phase angle φ corresponds to the angle between the initial plane of polarization and the optical axis of the $\lambda/4$ plate or the polarization plane of the Fresnel rhomb.

For optical inter-band excitation a cw-Ti:Sapphire laser was used providing radiation of $\lambda = 0.777$ μm with about 100 mW power. In order to extract the helicity dependent current the linearly polarized laser beam was transmitted through a photoelastic modulator which yields a periodically oscillating polarization between σ_+ and σ_- [29].

Samples were studied at room temperature or mounted in an optical cryostat which allowed the variation of temperature in the range of 4.2 K to 293 K. The photocurrent j_x was measured in the unbiased structures via the voltage drop across a 50 Ω load resistor in a closed circuit configuration [10] (see Fig. 9c). The current in the case of the excitation by visible radiation was recorded by a lock-in amplifier in phase with the photoelastic modulator.

The experiments on the spin-galvanic effect, which require an external magnetic field, were performed at room temperature in a conventional electromagnet with the magnetic field up to 1 T and at 4.2 K using a superconducting split-coil magnet with B up to 3 T.

4 Experimental results and discussion

4.1 Spin polarization induced circular photogalvanic effect

4.1.1 General features

With illumination of QW structures by polarized radiation a current signal proportional to the helicity P_{circ} has been observed in unbiased samples [10, 20, 23, 43]. The irradiated QW structure represents a current source wherein the current flows in the QW. Fig. 9 shows measurements of the voltage drop across a 50 Ω load resistor in response to 100 ns laser pulses at $\lambda = 10.6$ μm . Signal traces are plotted in Fig. 9a for right- and in Fig. 9b for left-handed circular polarization in comparison to a reference signal (see Fig. 9d) obtained from the fast photon-drag detector [104,105]. The signal follows the temporal structure of the applied laser pulses. In Fig. 10 the current is shown as a function of the phase angle φ . The current signal assumes a maximum at circular polarized radiation and changes sign if the polarization is switched from σ_+ to σ_- . In the case of linearly polarized radiation corresponding to $\varphi = 0^\circ$ or 90° the current vanishes. The radiation induced current and its characteristic helicity dependence reveals that we are dealing with the circular photogalvanic effect. The effect is quite general and has been observed in all samples in the temperature range of 4.2 K to 293 K and in a wide spectral range.

In (001)-oriented samples a helicity dependent signal is only observed under oblique incidence [20,21,23]. For light propagating along $\langle 110 \rangle$ direction the photocurrent flows perpendicular to the wavevector of the incident light (see Fig. 10, upper plate). This observation is in accordance to Eqs. (14). For illumination along a cubic axis $\langle 100 \rangle$ both a transverse and longitudinal circular photogalvanic current are detected [22]. The presence of a transverse current in this geometric con-

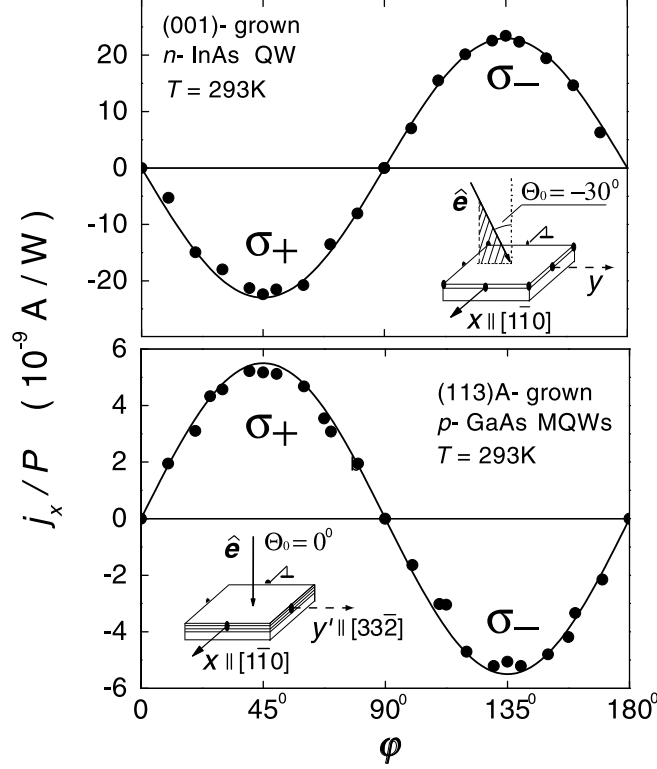


Figure 10: Photocurrent in QWs normalized by the light power P as a function of the phase angle φ defining helicity. Measurements are presented for $T = 293$ K and $\lambda = 76 \mu\text{m}$. The insets show the geometry of the experiment. Upper panel: oblique incidence of radiation with an angle of incidence $\Theta_0 = -30^\circ$ on n -type (001)-grown InAs/AlGaSb QWs (symmetry class C_{2v}). The current j_x is perpendicular to the direction of light propagation. Lower panel: normal incidence of radiation on p -type (113)A-grown GaAs/AlGaAs QWs (symmetry class C_s). The current j_x flows along $[1\bar{1}0]$ -direction perpendicular to the mirror plane of C_s symmetry. Full lines show ordinate scale fits after Eqs. (14) and (15) for the top and lower panel, respectively.

figuration in all (001)-oriented samples, except miscut, investigated as yet unambiguously demonstrates that they belong to the symmetry class C_{2v} . Indeed, in such a geometry ($\hat{e}_x = \hat{e}_y = 1/\sqrt{2}$), the transverse effect is only allowed for the C_{2v} symmetry class and is forbidden for D_{2d} symmetry as it can be seen from Eqs. (13) and (14) and the discussion following. In samples grown on a (113)-GaAs surface or on (001)-miscut substrates representing the lower symmetry class C_s , the CPGE has been observed also under normal incidence of radiation [10, 20, 21, 23] as shown in the lower plate of Fig. 10. This is in contrast to (001)-oriented samples and in accordance to the phenomenological theory of the CPGE for C_s (see Eqs. (15)). For normal incidence in this symmetry the current always flows along the $[1\bar{1}0]$ -direction perpendicular to the plane of mirror reflection of the point group C_s . The solid lines in Fig. 10 are obtained from the phenomenological picture outlined above which perfectly describes the experimental observations.

In Fig. 11 we show the dependence of the photocurrent on the angle of incidence Θ_0 of the right-handed circularly polarized laser beam. For (001)-oriented samples (C_{2v} -symmetry) a variation of Θ_0 in the plane of incidence normal to x changes the sign of the current j_x at normal incidence, $\Theta_0=0$, as can be seen in the upper panel of Fig. 11. The lower panel of Fig. 11 displays the angular dependence for (113)-oriented quantum wells (C_s -symmetry). The currents measured as a function of the angle of incidence Θ_0 along any direction in the plane of (001)-oriented samples and along $x \parallel [1\bar{1}0]$ for (113)-oriented samples (Fig. 11) are in very good agreement with the phenomenological expressions Eqs. (14), (16), and (18) for C_{2v} and Eqs. (15), (17) and (18) for C_s symmetry. Both figures show experimental data compared to calculations which were fitted with one ordinate scaling parameter. The fact that j_x is an even function of Θ_0 for (113)-oriented samples means that in the sample under study the component $\gamma_{xz'}$ in Eqs. (15) of γ is much larger compared to $\gamma_{xy'}$.

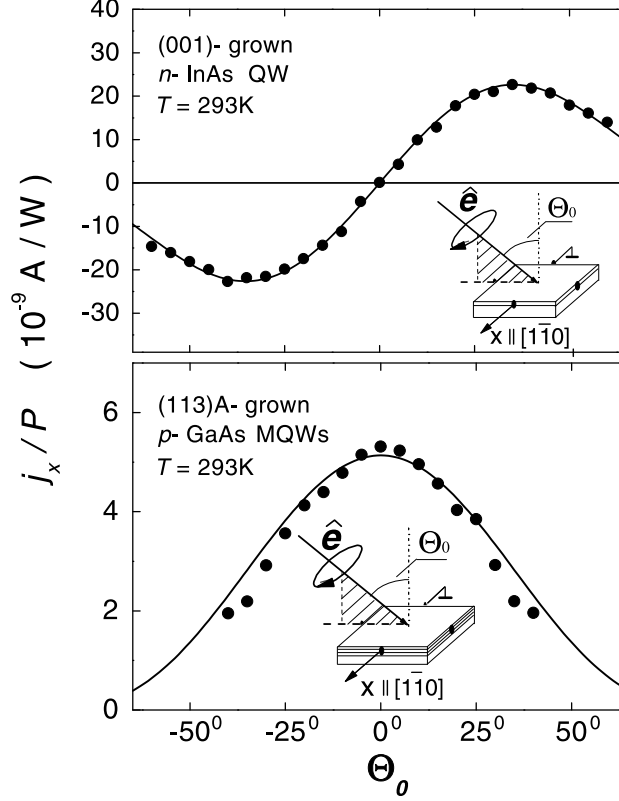


Figure 11: Photocurrent in QWs normalized by P as a function of the angle of incidence Θ_0 for right-handed circularly polarized radiation σ_+ measured perpendicular to light propagation ($T = 293$ K, $\lambda = 76$ μm). Upper panel: n -type (001)-grown InAs/AlGaSb QWs (C_{2v}). Lower panel: p -type (113)A-grown GaAs/AlGaAs QWs (C_s). Full lines show ordinate scale fits after Eqs. (14) (16) (upper plate) and (15) (17) (lower plate).

Microscopically CPGE can be the result of different optical absorption mechanisms like inter-band transitions, inter-subband transitions in QWs, Drude absorption etc. The CPGE at inter-band absorption (valence band to conduction band) has not been observed experimentally so far. A strong spurious photocurrent due to other mechanisms like the Dember effect, photovoltaic effects at contacts etc. mask the relatively weak CPGE. However application of polarization selective measurements, like modulation of polarization, should allow to extract the CPGE current. In the infrared range, where effects mentioned above vanish, the CPGE has been observed experimentally. In quantum well structures absorption of infrared radiation may occur at indirect intra-subband optical transitions (Drude absorption) and, for photon energies being in resonance with the energy distance between size quantized subbands, by direct transitions between these subbands.

4.1.2 Inter-subband transitions in n -type QWs

Absorption of radiation in the range of 9 μm up to 11 μm in n -type GaAs samples of QW widths 8.2 nm and 8.6 nm is dominated by resonant direct inter-subband optical transitions between the first and the second size-quantized subband. Fig. 12 shows the resonance behaviour of the absorption measured in GaAs QWs obtained by Fourier spectroscopy using a multiple-reflection waveguide geometry. Applying MIR radiation of the CO₂ laser, which causes direct transitions in GaAs QWs, a current signal proportional to the helicity P_{circ} has been observed at normal incidence in (113)-samples and at oblique incidence in (001)-oriented samples indicating the spin orientation induced circular photogalvanic effect [24]. In Fig. 12 the data are presented for a (001)-grown n -GaAs QW of 8.2 nm width measured at room temperature. It is seen that the current for both, left and right handed circular polarization, changes sign at a frequency $\omega = \omega_{\text{inv}}$. This inversion frequency ω_{inv} coincides with the frequency of the absorption peak. The peak frequency and

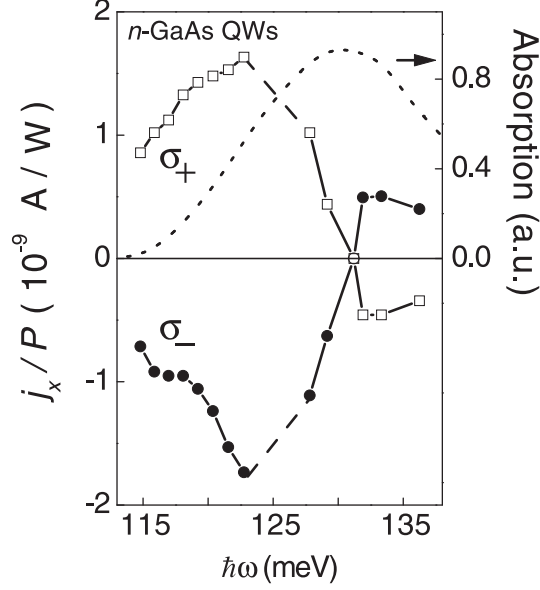


Figure 12: Photocurrent in QWs normalized by P as a function of the photon energy $\hbar\omega$. Measurements are presented for n -type (001)-grown GaAs/AlGaAs QWs of 8.2 nm width (symmetry class C_{2v}) at $T = 293$ K and oblique incidence of radiation with an angle of incidence $\Theta_0 = 20^\circ$. The absorption of the MIR laser radiation results in direct transitions between $e1$ and $e2$ subbands. The current j_x is perpendicular to the direction of light propagation. The dotted line shows the absorption measured using a Fourier spectrometer.

ω_{inv} depend on the sample width in agreement to the variation of the subband energy separation. Experimental results shown in Fig. 12, in particular the sign inversion of the spectral behaviour of the current, are in a good agreement with microscopic theory developed in [24] (see Eqs. (22) and (23)). The spectral sign inversion of the CPGE has also been detected in a (113)-oriented n -GaAs QW which belongs to the point group C_s . In this case the helicity dependent signal is observed in x -direction at normal incidence of radiation along z' .

The inversion of photon helicity driven current is a direct consequence of \mathbf{k} -linear terms in the band structure of subbands together with energy and momentum conservation as well as optical selection rules for direct optical transitions between size quantized subbands [24]. At large photon energy, $\hbar\omega > \varepsilon_{21}$, and for QWs of C_s symmetry excitation occurs at positive k_x resulting in a current j_x shown by an arrow in Fig. 2b. Decreasing of the photon frequency shifts the transition towards negative k_x and reverses the direction of the current. In the frame of this model the inversion of sign of the current takes place at the photon energy $\hbar\omega_{inv}$ corresponding to optical transitions from the band minima. This shift of ω_{inv} away from the frequency of peak absorption cannot be resolved in experiment on currently available samples because of the broadening of the absorption [24]. Similar arguments hold for C_{2v} symmetry (relevant for (001)-oriented samples) under oblique incidence (see Fig. 5a) although the simple selection rules are no longer valid [14, 106]. Due to selection rules the absorption of circularly polarized radiation is spin-conserving but the rates of inter-subband transitions are different for electrons with the spin oriented co-parallel and anti-parallel to the in-plane direction of light propagation [91]. The asymmetric distribution of photo-excited electrons results in a current which is caused by these spin-conserving but spin-dependent transitions [24].

4.1.3 Inter-subband transitions in p -type QWs

The helicity dependent current of the spin orientation induced CPGE has also been observed in p -type GaAs QWs due to transitions between heavy-hole ($hh1$) and light-hole ($lh1$) subbands demonstrating spin orientation of holes (see Fig. 10, lower plate) [10, 20, 38]. QWs with various widths in the range of 4 to 20 nm were investigated. For direct inter-subband transitions photon energies between 35 meV and 8 meV of FIR radiation corresponding to these QW widths were

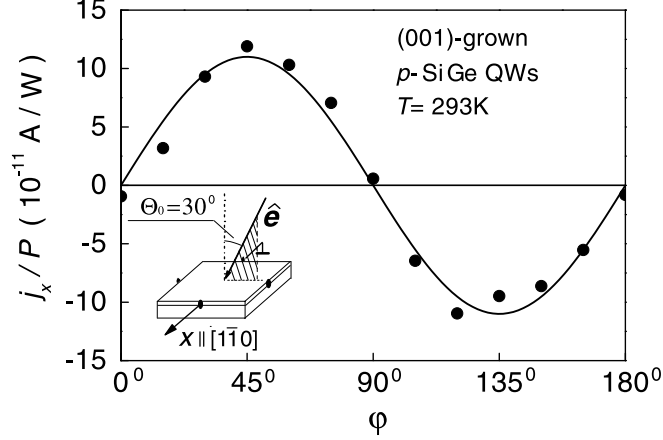


Figure 13: Photogalvanic current j_x normalized by P in (001)-grown and asymmetrically doped SiGe QWs and measured at room temperature as a function of the phase angle φ . The data were obtained under oblique incidence of irradiation at $\lambda = 10.6 \mu\text{m}$. The full line is fitted after Eqs. (14). The inset shows the geometry of the experiment.

applied. Due to different effective masses of light and heavy holes the absorption does not show narrow resonances. Cooling the sample from room temperature to 4.2 K leads to a change of sign of spin orientation induced CPGE but the $\sin 2\varphi$ dependence is retained [10]. This temperature dependent change of sign of the photogalvanic current, which was also observed in n -type samples at direct transitions, may be caused by the change of scattering mechanism from impurity scattering to phonon assisted scattering (see section 2.2.3).

4.1.4 Intra-subband transitions in QWs

Optical absorption caused by indirect transitions in n -type samples have been obtained applying FIR radiation covering the range of $76 \mu\text{m}$ to $280 \mu\text{m}$ corresponding to photon energies from 16 meV to 4.4 meV. The experiments were carried out on GaAs [20,21], InAs [20] and semimagnetic ZnBeMnSe [43] QWs. The energy separation between $e1$ and $e2$ size-quantized subbands of those samples is much larger than the FIR photon energies used here. Therefore the absorption is caused by indirect intra-subband optical transitions. With illumination of (001)-grown QWs at oblique incidence of FIR radiation a current signal proportional to the helicity P_{circ} has been observed (see Fig. 10, upper plate) showing that Drude absorption of a 2D electron gas results in spin orientation and the CPGE. Spin orientation induced CPGE at intra-subband absorption was also observed in p -type samples at long wavelengths [10,21,23], where the photon energies are smaller than the energy separation between the first heavy-hole and the first light-hole subbands.

4.1.5 Spin orientation induced CPGE in SiGe QWs

In symmetrically (001)-grown and symmetrically doped SiGe QWs no photogalvanic current has been observed as expected from the presence of inversion symmetry in both materials. However, in non-symmetric QWs as described in section 3.1, spin orientation induced CPGE has been observed being caused by the Rashba spin-orbit coupling due to built-in potential gradient in the QWs [23, 107]. Spin orientation induced CPGE is most clearly seen at $hh1-lh1$ inter-subband absorption in (001)-oriented p -type QWs. With illumination by MIR radiation of the CO₂ laser a current signal proportional to the helicity P_{circ} is observed under oblique incidence (Fig. 13). For irradiation along $\langle 110 \rangle$ as well as along $\langle 100 \rangle$ crystallographic directions the photocurrent flows perpendicular to the propagation direction of the incident light. Therefore only a transverse CPGE was observed. It means that the effect of a Dresselhaus-like \mathbf{k} -linear term yielding a longitudinal effect for $\langle 100 \rangle$ is negligible [107]. The wavelength dependence of the photocurrent obtained between $9.2 \mu\text{m}$ and $10.6 \mu\text{m}$ corresponds to the spectral behaviour of direct inter-subband absorption between the lowest heavy-hole and light-hole subbands measured in transmission (see Fig. 14).

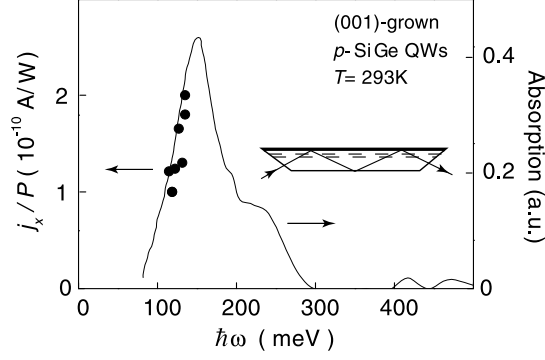


Figure 14: Spectral dependence of spin orientation induced CPGE (full dots) in (001)-grown and asymmetrically doped SiGe QWs due to direct transitions between $hh1$ and $lh1$ valence subbands at room temperature. The full line shows the absorption spectrum obtained at 10 K. The absorption has been determined by transmission measurements making use of a multiple-reflection waveguide geometry shown in the inset.

In the FIR range a more complicated dependence of the current as a function of helicity has been observed. In (001)-grown asymmetric quantum wells as well as in (113)-grown samples the dependence of the current on the phase angle φ may be described by the sum of two terms, one of them is $\propto \sin 2\varphi$ and the other $\propto \sin 2\varphi \cdot \cos 2\varphi$. In Fig. 15 experimental data and a fit to these functions are shown for a step bunched (001)-grown SiGe sample. The first term is due to the spin orientation induced CPGE and the second term is caused by a linear photogalvanic effect [23] which will be discussed later (see section 5.1, Eqs. (42)). For circularly polarized radiation the linear photogalvanic term $\sin 2\varphi \cdot \cos 2\varphi$ is equal to zero and the observed current is due to spin orientation induced CPGE only. We would like to point out that, in agreement to symmetry, the same term may also be present in zinc-blende structure based QWs but has not yet been detected. CPGE and LPGE have different microscopic physical mechanisms. Variation of material parameters, excitation wavelengths, and temperature may change the relative strengths of these effects. For both spectral ranges, MIR and FIR, the angle of incidence dependence of CPGE in SiGe structures is the same as shown above for zinc-blende structure based materials.

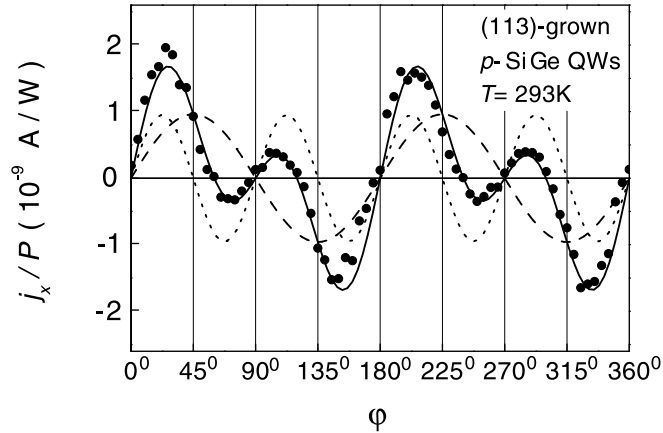


Figure 15: Photogalvanic current in (113)-grown SiGe QWs normalized by the light power P as a function of the phase angle φ . The results were obtained at $\lambda = 280 \mu\text{m}$ under normal incidence of irradiation at room temperature. The full line is fitted after left equations of Eqs. (15) and (42) corresponding to CPGE and LPGE, respectively. Broken and dotted lines show $j_x \propto \sin 2\varphi$ and $j_x \propto \sin 2\varphi \cdot \cos 2\varphi$, respectively.

The experimental results described so far are due to an imbalance of photoexcited spin polarized electrons in \mathbf{k} -space yielding the circular photogalvanic effect. After momentum relaxation of the photoexcited carriers spin orientation induced CPGE vanishes, however, a spin orientation may

still be present if the spin relaxation time is longer than the momentum relaxation time. In such a case the spin-galvanic effect may contribute to the total current. In the next section we present experimental results demonstrating a pure spin-galvanic effect without admixture of spin orientation induced CPGE.

please replace the list of references by part II
starting with the page number 28

Acknowledgement

The authors thank E.L. Ivchenko, V.V. Bel'kov, L.E. Golub, S.N. Danilov and Petra Schneider for many discussions and helpful comments on the present manuscript. We are also indebted to G. Abstreiter, V.V. Bel'kov, M. Bichler, J. DeBoeck, G. Borghs, K. Brunner, S.N. Danilov, J. Eroms, E.L. Ivchenko, S. Giglberger, P. Grabs, L.E. Golub, T. Humbs, J. Kainz, H. Ketterl, B.N. Murdin, Petra Schneider, D. Schuh, M. Sollinger, S.A. Tarasenko, L. Molenkamp, R. Newmann, V.I. Perel, C.R. Pidgeon, P.J. Phillips, U. Rössler, W. Schoepe, D. Schowalter, G. Schmidt, V.M. Ustinov, L.E. Vorobjev, D. Weiss, W. Wegscheider, D.R. Yakovlev, I.N. Yassievich, and A.E. Zhukov, for long standing cooperation during the work on spin photocurrents. We gratefully acknowledge financial support by the Deutsche Forschungsgemeinschaft (DFG), the Russian Foundation for Basic Research (RFBR) and the NATO Linkage Grant which made this work possible.

References

- [1] *Semiconductor Spintronics and Quantum Computation*, eds. D.D. Awschalom, D. Loss, and N. Samarth, in the series *Nanoscience and technology*, eds. K. von Klitzing, H. Sakaki, and R. Wiesendanger (Springer, Berlin, 2002).
- [2] Y.A. Bychkov, and E.I. Rashba, Pis'ma ZhETF **39**, 66 (1984) [Sov. JETP Lett. **39**, 78 (1984)].
- [3] *Optical orientation*, F. Meier, and B.P. Zakharchenya, Eds. (Elsevier Science Publ., Amsterdam, 1984).
- [4] D. Hägele, M. Oestreich, W.W. Rühle, N. Nestle, and K. Eberl, Appl. Phys. Lett. **73**, 1580 (1998).
- [5] J.M. Kikkawa, and D.D. Awschalom, Nature **397**, 139 (1999).
- [6] A. Hirohata, Y.B. Xu, C.M. Guertler, and A.C. Bland, J. Appl. Phys. **85**, 5804 (1999).
- [7] N.S. Averkiev, and M.I. D'yakonov, Fiz. Tekh. Poluprov. **17**, 629 (1983) [Sov. Phys.Semicond. **17**, 393 (1983)].
- [8] M.I. D'yakonov, V.I. Perel', Pis'ma ZhETF **13**, 206 (1971) [Sov. JETP Lett. **13**, 144 (1971)].
- [9] A.A. Bakun, B.P. Zakharchenya, A.A. Rogachev, M.N. Tkachuk, and V.G. Fleisher, Pis'ma ZhETF **40**, 464 (1984) [Sov. JETP Lett. **40**, 1293 (1984)].
- [10] S.D. Ganichev, E.L. Ivchenko, H. Ketterl, W. Prettl, and L.E. Vorobjev, Appl. Phys. Lett. **77**, 3146 (2000).
- [11] E.L. Ivchenko, and G.E. Pikus, in *Problems of Modern Physics* (in Russian), ed. V.M. Tuchkevich and V.Ya. Frenkel, Leningrad, Nauka, 1980, p.275 [English translation: *Semiconductor Physics*, ed. V.M. Tuchkevich and V.Ya. Frenkel, Cons. Bureau, New York, 1986, p. 427].
- [12] V.I. Belinicher, and B.I. Sturman, Usp. Fiz. Nauk **130**, 415 (1980) [Sov. Phys. Usp. **23**, 199 (1980)].
- [13] B.I. Sturman, and V.M. Fridkin, *The Photovoltaic and Photorefractive Effects in Non-Centrosymmetric Materials*, Gordon and Breach Science Publishers, New York, 1992.
- [14] E.L. Ivchenko, and G.E. Pikus, *Superlattices and Other Heterostructures. Symmetry and Optical Phenomena*, (Springer, Berlin 1997).

- [15] E.L. Ivchenko, and G.E. Pikus, Pis'ma ZhETF **27**, 640 (1978) [Sov. JETP Lett. **27**, 604 (1978)].
- [16] V.I. Belinicher, Phys. Lett. A **66**, 213 (1978).
- [17] V.M. Asnin, A.A. Bakun, A.M. Danishevskii, E.L. Ivchenko, G.E. Pikus, and A.A. Rogachev, Pis'ma ZhETF **28**, 80 (1978) [Sov. JETP Lett. **28**, 74 (1978)].
- [18] V.M. Asnin, A.A. Bakun, A.M. Danishevskii, E.L. Ivchenko, G.E. Pikus, and A.A. Rogachev, Solid State Commun. **30**, 565 (1979).
- [19] N.S. Averkiev, V.M. Asnin, A.A. Bakun, A.M. Danishevskii, E.L. Ivchenko, G.E. Pikus, A.A. Rogachev, Fiz. Tekh. Poluprov. **18**, 639; 648 (1984) [Sov. Phys. Semicond. **18**, 397; 402 (1984)].
- [20] S.D. Ganichev, E. L. Ivchenko, S.N. Danilov, J. Eroms, W. Wegscheider, D. Weiss, and W. Prettl, Phys. Rev. Lett. **86**, 4358 (2001).
- [21] S.D. Ganichev, E.L. Ivchenko, and W. Prettl, Physica E **14**, 166 (2002).
- [22] S.D. Ganichev, Proceed. of ICPS-26, to be published.
- [23] S.D. Ganichev, U. Rössler, W. Prettl, E.L. Ivchenko, V.V. Bel'kov, R. Neumann, K. Brunner, and G. Abstreiter, Phys. Rev. B **66**, 75328 (2002).
- [24] S.D. Ganichev, V.V. Bel'kov, Petra Schneider, E.L. Ivchenko, S.A. Tarasenko, D. Schuh, W. Wegscheider, D. Weiss, and W. Prettl, submitted to Phys. Rev. B (cond-mat/0303054).
- [25] L.E. Golub, Physica E, to be published (cond-mat/0208295).
- [26] L.E. Golub, Phys. Rev. B, to be published.
- [27] E.L. Ivchenko, Yu.B. Lyanda-Geller, and G.E. Pikus, Pis'ma ZhETF **50**, 156 (1989) [Sov. JETP Lett. **50**, 175 (1989)].
- [28] E.L. Ivchenko, Yu.B. Lyanda-Geller, and G.E. Pikus, ZhETF **98**, 989 (1990) [Sov. Phys. JETP **71**, 550 (1990)].
- [29] S.D. Ganichev, E.L. Ivchenko, V.V. Bel'kov, S.A. Tarasenko, M. Sollinger, D. Weiss, W. Wegscheider, and W. Prettl, *Nature* (London) **417**, 153 (2002).
- [30] S.D. Ganichev, E.L. Ivchenko, V.V. Bel'kov, S.A. Tarasenko, M. Sollinger, D. Schowalter, D. Weiss, W. Wegscheider, and W. Prettl, J. of Supercond.: Incorporating Novel Magn. **16**, 369 (2003) (cond-mat/0301390).
- [31] S.D. Ganichev, Petra Schneider, V.V. Bel'kov, E.L. Ivchenko, S.A. Tarasenko, W. Wegscheider, D. Weiss, D. Schuh, D.G. Clarke, M. Merrick, B.N. Murdin, P. Murzyn, P.J. Phillips, C.R. Pidgeon, E.V. Berezulin, and W. Prettl, submitted to Phys. Rev. B. (cond-mat/0303193).
- [32] R.D.R. Bhat, and J.E. Sipe, Phys. Rev. Lett. **85**, 5432 (2000).
- [33] M.J. Stevens, A.L. Smirl, R.D.R. Bhat, J.E. Sipe, and H.M. van Driel, J. Appl. Phys. **91**, 4382 (2002).
- [34] M.V. Entin, Fiz. Tekh. Poluprov. **23**, 1066 (1989) [Sov. Phys. Semicond. **23**, 664 (1989)].
- [35] L.I. Magarill, Physica E **9**, 652 (2001).
- [36] S.D. Ganichev, H. Ketterl, and W. Prettl, Physica B **272**, 464 (1999).
- [37] S.D. Ganichev, V.V. Bel'kov, S.N. Danilov, E.L. Ivchenko, H. Ketterl, L.E. Vorobjev, M. Bichler, W. Wegscheider, and W. Prettl, Physica E **10**, 52 (2001).

- [38] S.D. Ganichev, S.N. Danilov, V.V. Bel'kov, E.L. Ivchenko, M. Bichler, W. Wegscheider, D. Weiss, and W. Prettl, Phys. Rev. Lett. **88**, 057401-1 (2002).
- [39] S.D. Ganichev, S.N. Danilov, M. Sollinger, D. Weiss, W. Wegscheider, W. Prettl, V.V. Bel'kov, and E.L. Ivchenko, MRS Symp. Proc. **690**, eds. T.J. Klemmer, J.S. Sun, A. Fert, and J. Bass, F1.2.1 (2001).
- [40] S.A. Tarasenko, E.L. Ivchenko, V.V. Bel'kov, S.D. Ganichev, D. Schowalter, Petra Schneider, M. Sollinger, W. Prettl, V.M. Ustinov, A.E. Zhukov, and L. E. Vorobjev, Proceed. of ICPS-26, to be published (cond-mat/0301393).
- [41] S.A. Tarasenko, E.L. Ivchenko, V.V. Bel'kov, S.D. Ganichev, D. Schowalter, Petra Schneider, M. Sollinger, and W. Prettl, V.M. Ustinov, A.E. Zhukov, and L.E. Vorobjev, Journal of Supercond.: Incorporating novel Magn. **16**, 419 (2003) (cond-mat/0301388).
- [42] S.D. Ganichev, H. Ketterl, and W. Prettl, Int. J. Infared and MM Waves, to be published.
- [43] S.D. Ganichev, M. Sollinger, W. Prettl, D.R. Yakovlev, P. Grabs, G. Schmidt, L. Molenkamp, and E.L. Ivchenko, Verhandl. DPG (VI) **36**, 1/170 (2001).
- [44] D. Stein, K. von Klitzing, and G. Weimann, Phys. Rev. Lett. **51**, 130 (1983).
- [45] H.L. Stormer, Z. Schlesinger, A. Chang, D.C. Tsui, A.C. Gossard, and W. Wiegmann, Phys. Rev. Lett. **51**, 126 (1983).
- [46] M.I. D'yakonov, and V.Yu. Kachorovskii, Fiz. Tekh. Poluprov. **20**, 178 (1986) [Sov. Phys. Semicond. **20**, 110 (1986)].
- [47] N.S. Averkiev, L.E. Golub, and M. Willander, J. Phys.: Condens. Matter **14**, R271 (2002).
- [48] A. Voskoboynikov, S.S. Liu, and C.P. Lee, Phys. Rev. B **58**, 15397 (1998).
- [49] E.A. de Andrada e Silva, G.C. La Rocca, Phys. Rev. B **59**, 15583 (1999).
- [50] T. Koga, J. Nitta, H. Takayanagi, and S. Datta, Phys. Rev. Lett. **88**, 126601 (2002).
- [51] V.I. Perel', S.A. Tarasenko, I.N. Yassievich, S.D. Ganichev, V.V. Bel'kov, and W. Prettl, submitted to Phys. Rev. B. (cond-mat/ 0301098).
- [52] V.K. Kalevich, and V.L. Korenev, Pis'ma ZhETF **52**, 859 (1990) [Sov. JETP Lett. **52**, 230 (1990)].
- [53] J. Nitta, T. Akazaki, and H. Takayanagi, Phys. Rev. Lett. **78**, 1335 (1997).
- [54] J.P. Lu, J.B. Yau, S.P. Shukla, M. Shayegan, L. Wissinger, U. Rössler, and R. Winkler, Phys. Rev. Lett. **81**, 1282 (1998).
- [55] J.P. Heida, B.J. van Wees, J.J. Kuipers, T.M. Klapwijk, G. Borghs, Phys. Rev. B **57**, 11911 (1998).
- [56] C.-M. Hu, J. Nitta, T. Akazaki, H. Takayanagi, J. Osaka, P. Pfeffer, and W. Zawadzki, Phys. Rev. B **60**, 7736 (1999).
- [57] G. Salis, Y. Kato, K. Ensslin, D.C. Driscoll, A.C. Gossard, and D.D. Awschalom, Nature **414**, 619 (2001).
- [58] J. H. Smet, R. A. Deutschmann, F. Ertl, W. Wegscheider, G. Abstreiter, K. von Klitzing, Nature **415**, 281 (2002).
- [59] F.T. Vas'ko, and N.A. Prima, Fiz. Tverd. Tela **21**, 1734 (1979) [Sov. Phys. Solid State **21**, 994 (1979)].

- [60] U. Rössler, Solid State Comm. **49**, 943 (1984).
- [61] M. Cardona, N.E. Christensen, G. Fasol, Phys. Rev. B **38**, 1806 (1988).
- [62] G. Lommer, F. Malcher, U. Rössler, Phys. Rev. Lett. **60**, 728 (1988).
- [63] J. Luo, H. Munekata, F.F. Fang, and P.J. Stiles, Phys. Rev. B **38**, 10142 (1988).
- [64] B. Das, D.C. Miller, S. Datta, R. Reifenberger, W.P. Hong, P.K. Bhattacharya, J. Singh, M. Jaffe, Phys. Rev. B **39**, 1411 (1989).
- [65] J. Luo, H. Munekata, F.F. Fang, and P.J. Stiles, Phys. Rev. B **41**, 7685 (1990).
- [66] Yu.L. Ivanov, P.S. Kop'ev, S.D. Suchalkin, and V.M. Ustinov, Pis'ma ZhETP **53**, 470 (1991) [Sov. JETP Lett. **53**, 493 (1991)]
- [67] P.D. Dresselhaus, C.M. A. Papavassiliou, R.G. Wheeler, R.N. Sacks, Phys. Rev. Lett. **68**, 106 (1992).
- [68] E.A. de Andrada e Silva, Phys. Rev. B **46**, 1921 (1992).
- [69] R.V. Santos, and M. Cardona, Phys. Rev. B **72**, 432 (1994).??
- [70] E.A. Andrada e Silva, G.C. La Rocca, and F. Bassani, Phys. Rev. B **50**, 8523 (1994).
- [71] B. Jusserand, D. Richards, G. Allan, C. Priester, and B. Etienne, Phys. Rev. B **51**, 4707 (1995).
- [72] P. Pfeffer, and W. Zawadski, Phys. Rev. B **52**, R14332 (1995).
- [73] E.L. Ivchenko, A.Yu. Kaminski, and U. Rössler, Phys. Rev. B **54**, 5852 (1996).
- [74] G. Engels, J. Lange, Th. Schäpers, and H. Lüth, Phys. Rev. B **55**, R1958 (1997).
- [75] E.A. Andrada e Silva, G.C. La Rocca, and F. Bassani, Phys. Rev. B **55**, 16293 (1997).
- [76] D. Grundler, Phys. Rev. Lett. **84**, 6074 (2000).
- [77] P.R. Hammar, M. Johnson, Phys. Rev. B **61**, 7207 (2000).
- [78] J.A. Majewski, P. Vogl, P. Lugli, Proc. of the 25th Int. Conf. of Physics of Semiconductors (ICPS), Eds. N. Miura, T. Ando, Springer Verlag Berlin, 791 (2001).
- [79] Z. Wilamowski, W. Jantsch, H. Malissa, and U. Rössler, Phys. Rev. B **66**, 195315 (2002).
- [80] S.A. Tarasenko, and N.S. Averkiev, Pis'ma ZhETF **75**, 669 (2002) [Sov. JETP Lett. **75**, 552 (2002)].
- [81] O. Krebs, and P. Voisin, Phys. Rev. Lett. **77**, 1829 (1996).
- [82] T. Guettler, A.L.C. Triques, L. Vervoort, R. Ferreira, Ph. Roussignol, P. Voisin, D. Rondi, and J.C. Harmand, Phys. Rev. B **58**, R10179 (1998).
- [83] O. Krebs, D. Rondi, J.L. Gentner, L. Goldstein, and P. Voisin, Phys. Rev. Lett. **80**, 5770 (1998).
- [84] A.A. Toropov, E. L.Ivchenko, O. Krebs, S. Cortez, P. Voisin, and J.L. Gentner, Phys. Rev. B **63**, 035302 (2000).
- [85] J.T. Olesberg, W.H. Lau, M. Flatte, C.Yu.E. Altunkaya, E.M. Shaw, T.C. Hasenberg, and T. Bogges, Phys. Rev. B **64**, 201301 (2001).
- [86] U. Rössler, and J. Kainz, Solid State Comm. **121**, 313 (2002).

- [87] L.E. Golub, and E.L. Ivchenko, to be published (cond-mat/0302308).
- [88] G. Dresselhaus, Phys. Rev. **100**, 580 (1955).
- [89] E.I. Rashba, Fiz. Tverd. Tela **2** 1224 (1960) [Sov Phys. Sol. State **2**, 1109 (1960)].
- [90] S. Datta, B. Das, Appl. Phys. Lett. **56**, 665 (1990).
- [91] E.L. Ivchenko, and S.A. Tarasenko, JETP, to be published.
- [92] A. Haché, Y. Kostoulas, R. Atanasov, J.L.P. Hudges, J.E. Sipe, and H.M. van Driel, Phys. Rev. Lett. **78**, 306 (1997).
- [93] A.G. Aronov, and Yu. B. Lyanda-Geller, Pis'ma ZhETF **50**, 398 (1989) [Sov. JETP Lett. **50**, 431 (1990)].
- [94] V.M. Edelstein, Solid State Comm. **73**, 233 (1990).
- [95] R.R. Parson, Can. J. Phys. **49**, 1850 (1971).
- [96] W. Hanle, Zeitschrift für Physik **30**, 93 (1924).
- [97] A.V. Andrianov, and I.D. Yaroshetskii, Pis'ma ZhETF **40**, 131 (1984) [Sov. JETP Lett. **40**, 882 (1984)].
- [98] E.L. Ivchenko, Yu.B. Lyanda-Geller, and G.E. Pikus, Solid State Commun. **69**, 663 (1989).
- [99] M. Behet, S. Nemeth, J. DeBoeck, G. Borghs, J. Tümmeler, J. Woitok, J. Geurts Semicond. Sci. Techn. **13**, 428 (1998).
- [100] R. Fiederling M. Keim, G. Reuscher, W. Ossau, G. Schmidt, A. Waag, and L.W. Molenkamp, Nature **402**, 787 (1999).
- [101] S.D. Ganichev, Physica B **273-274**, 737 (1999).
- [102] S.D. Ganichev, I.N. Yassievich, and W. Prettl, J. Phys.: Condens. Matter **14**, R1263 (2002).
- [103] G.M.H. Knippels, X. Yan, A.M. MacLeod, W.A. Gillespie, M. Yasumoto, D. Oepts and A.F.G. van der Meer, Phys. Rev. Lett. **83**, 1578 (1999).
- [104] S.D. Ganichev, Ya.V. Terent'ev, and I.D. Yaroshetskii, Pis'ma Zh. Tekh. Phys. **11**, 46 (1985) Sov. Tech. Phys. Lett. **11**, 20 (1985).
- [105] E.V. Beregin, S.D. Ganichev, I.D. Yaroshetskii, P.T. Lang, W. Schatz, and K.F. Renk, Proc. SPIE **1362-2**, ed by M. Razeghi, 853 (1990).
- [106] R.J. Warburton, C. Gauer, A. Wixforth, and J.P. Kotthaus, B. Brar, and H. Kroemer, Phys. Rev. B **53**, 7903 (1996).
- [107] V.V. Bel'kov, S.D. Ganichev, Petra Schneider, D. Schowalter, U. Rössler, W. Prettl, E. L. Ivchenko, R. Neumann, K. Brunner, and G. Abstreiter, J. of Supercond.: Incorporating Novel Magn. **16**, 419 (2003) (con-mat/0301389).
- [108] X. Marie, T. Amand, P. Le Jeune, M. Paillard, P. Renucci, L.E. Golub, V.D. Dymnikov, and E.L. Ivchenko, Phys. Rev. B **60**, 5811 (1999).
- [109] G. Lampel, Phys. Rev. Lett. **20**, 491 (1968).
- [110] A.I. Ekimov, and V.I. Safarov, Pis'ma ZhETF **12**, 293 (1970) [Sov. JETP Lett. **12**, 198 (1970)].
- [111] B.I. Zakharchenya, V.G. Fleisher, R.I. Dzhirov, Yu.P. Veshchunov, and I.B. Rusanov, Pis'ma ZhETF **13**, 195 (1971) [Sov. JETP Lett. **13**, 137 (1971)].

- [112] A.M. Danishevskii, E.L. Ivchenko, S.F. Kochegarov, and V.K. Subashiev, Fiz. Tverd. Tela **27**, 710 (1985) [Sov. Phys. Solid State **27**, 439 (1985)].
- [113] R. Ferreira, and G. Bastard, Phys. Rev. B. **43**, 9687 (1991).
- [114] L.E. Vorobjev, D.V. Donetskii, and L.E. Golub, Pis'ma ZhETF **63**, 977 (1996) [Sov. JETP Lett. **63**, 981 (1996)].
- [115] Petra Schneider, S.D. Ganichev, J. Kainz, U. Rössler, W. Wegscheider, D. Weiss, W. Prettl, V.V. Bel'kov, L.E. Golub, D. Schuh, phys.stat. sol. **a**, to be published (cond-mat/0303056).
- [116] J. Shah, *Ultrafast spectroscopy of semiconductor nanostructures*, Springer (1999), pp. 243-261.
- [117] L. Viña, J. Phys.: Condens. Matter **11**, 5929 (1999).
- [118] I.D. Yaroshetskii, and S.M. Ryvkin, in *Problems of Modern Physics* (in Russian), ed. V.M. Tuchkevich and V.Ya. Frenkel, Leningrad, Nauka, 1980, p.173 [English translation: *Semiconductor Physics*, ed. V.M. Tuchkevich and V.Ya. Frenkel, Cons. Bureau, New York, 1986, p. 249].
- [119] A.F. Gibson, and M.F. Kimmitt *Photon Drag Detection in: Infrared and Millimeter Waves*, ed. by K.J. Button, N.Y., **3**, 182 (1980).
- [120] A.M. Glass, D. von der Linde, and T.J. Negran, Appl. Phys. Lett. **25**, 233 (1974).
- [121] V.I. Belinicher, V.K. Malinovskii, and B.I. Sturman, ZhETF **73**, 692 (1977) [Sov. JETP Lett. **46**, 362 (1977)].
- [122] L.I. Magarill, and M.V. Entin, Poverchnost' **1**, 74 (1982) [Sov. Surface **1**, 74 (1982)].
- [123] G.M. Gusev, Z.D. Kvon, L.I. Magarill, A.M. Palkin, V.I. Sozinov, O.A. Shegai, and M.V. Entin, Pis'ma ZhETP **46**, 28 (1987) [Sov. JETP Lett. **46**, 33 (1987)].
- [124] H. Schneider, S. Ehret, C. Schönbein, K. Schwarz, G. Bihlmann, J. Fleissner, G. Tränkle, and G. Böhm, Superlatt. Microstruct. **23**, 1289 (1998).
- [125] R. von Baltz and W. Kraut, Phys. Lett. A **79**, 364 (1980).
- [126] V.I. Belinicher, E.L. Ivchenko, and B.I. Sturman, ZhETF **83**, 649 (1982) [Sov. JETP **56**, 359 (1982)].
- [127] E.L. Ivchenko, Yu.B. Lyanda-Geller, and G.E. Pikus, Fiz. Tekh. Poluprov. **18**, 93 (1984) [Sov. Phys. Semicond. **18**, 55 (1984)].
- [128] A.V. Andrianov, E.V. Beregulín, S.D. Ganichev, K.Yu. Gloukh, and I.D. Yaroshetskii, Pis'ma Zh. Tekh. Fiz. **14**, 1326 (1988) Sov. Tech. Phys. Lett. **14**, 580 (1988).
- [129] C. Schönbein, H. Schneider, G. Bihlmann, K. Schwarz, and P. Koidl, Appl. Phys. Lett. **68**, 973 (1995).
- [130] A.M. Danishevskii, A.A. Kastal'skii, S.M. Ryvkin, and I.D. Yaroshetskii, ZhETF **58**, 544 (1970) [Sov. JETP **31**, 292 (1970)].
- [131] A.F. Gibson, M.F. Kimmit, and A.C. Walker, Appl. Phys. Lett. **17**, 75 (1970).
- [132] S. Luryi, Phys. Rev. Lett. **58**, 2263 (1987).
- [133] A.D. Wieck, H. Sigg, and K. Ploog, Phys. Rev. Lett. **64**, 463 (1990).
- [134] A.A. Grinberg and S. Luryi, Phys. Rev. B **38**, 87 (1988).

- [135] A.P. Dmitriev, S.A. Emel'yanov, S.V. Ivanov, P.S. Kop'ev, Ya.V. Terent'ev, and I.D. Yaroshetskii, Pis'ma ZhETF **54**, 460 (1991) [Sov. JETP Lett. **54**, 462 (1991)].
- [136] O. Keller, Phys. Rev. B **48**, 4786 (1993).
- [137] E.V. Beregulin, P.M. Voronov, S.V. Ivanov, P.S. Kop'ev, and I.D. Yaroshetskii, Pis'ma ZhETF **59**, 83 (1994) [Sov. JETP Lett. **59**, 85 (1994)].
- [138] F.T. Vasko, Phys. Rev. B **53**, 9576 (1996).
- [139] F.T. Vasko, and O. Keller, Phys. Rev. B. **58**, 15666 (1998).
- [140] H. Sigg, M.H. Kwakernaak, B. Margotte, D. Erni, P. van Son, and K. Köhler, Appl. Phys. Lett. **67**, 2827 (1995).
- [141] I. Žutić, J. Fabian, and S. Das Sarma, Appl. Phys. Lett. **79**, 1558 (2001).
- [142] I. Žutić, J. Fabian, and S. Das Sarma, Phys. Rev. Lett. **88**, 066603 (2002).
- [143] E.L. Ivchenko, B. Spivak, Phys. Rev. B **66**, 155404 (2002).